

Geohydraulics – fundamentals

Authors: Prof. Dr. habil. Heinz Konietzky
(TU Bergakademie Freiberg, Geotechnical Institute)

1	Introduction.....	2
2	Basic equations and parameters	3
3	Flow in fractured rock masses	15
4	Gas flow in geomaterials	20
5	Hydro-mechanical coupling	22
6	Permeability and porosity determination.....	28
7	Two-phase flow	30
8	Further geohydraulic problems.....	36
9	Literature	37

1 Introduction

Stress-strain behaviour of rock and rock masses is not only governed by mechanical properties of rock, but also influenced by hydro-mechanical coupling. If we include into our consideration soils, soft rocks / hard soils and rocks, the most important phenomena are flow through matrix and / or joints, effective stresses, buoyancy and seepage, consolidation, swelling / shrinkage, erosion, injection, liquefaction, capillarity, stress corrosion, solution processes, frost- and thaw effects as well as soil freezing. Depending on the considered process and the rock / soil type different approaches have to be applied. Fig. 1.1 gives an overview (not all-embracing) about different components from the mechanical and hydraulic point of view.

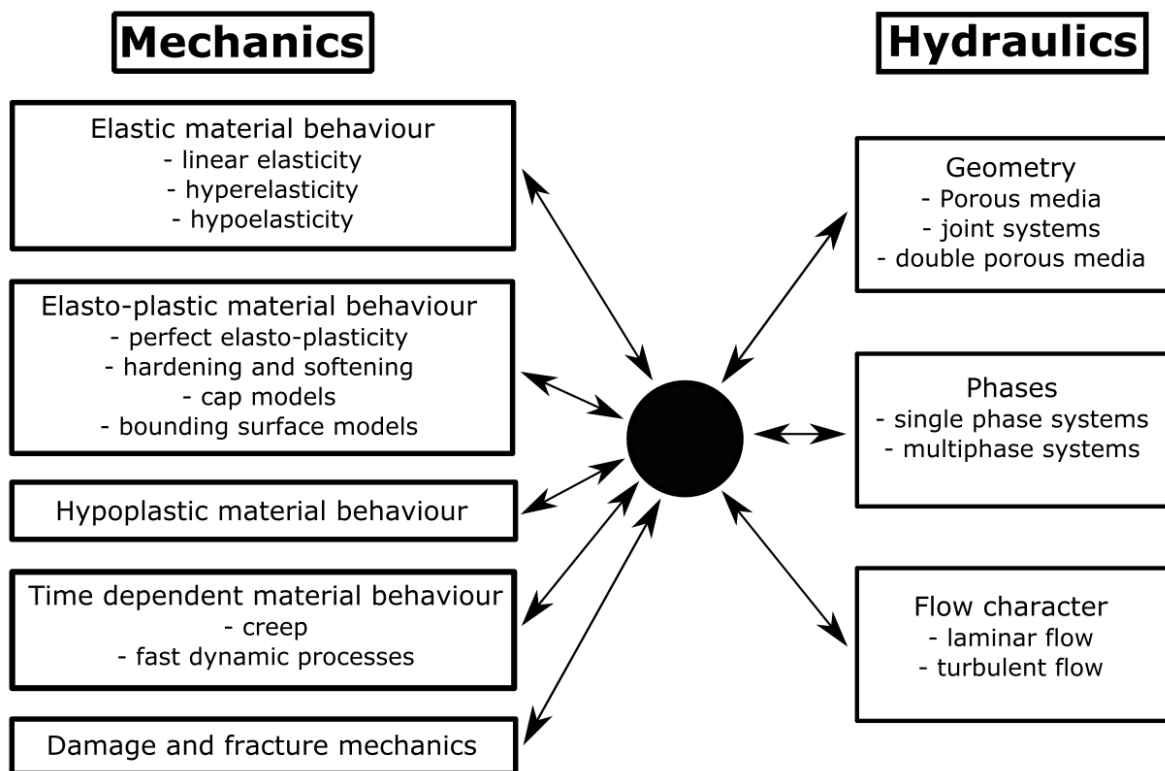


Fig. 1.1: Overview about mechanical and hydraulic components for HM-coupling.

2 Basic equations and parameters

Fluid flow can be characterised by the Navier-Stokes Equations:

$$\rho \left(\frac{\partial u}{\partial t} + u \frac{\partial u}{\partial x} + v \frac{\partial u}{\partial y} + w \frac{\partial u}{\partial z} \right) = -\frac{\partial p}{\partial x} + \rho g_x + \mu \left(\frac{\partial^2 u}{\partial x^2} + \frac{\partial^2 u}{\partial y^2} + \frac{\partial^2 u}{\partial z^2} \right) \quad (2.1)$$

$$\rho \left(\frac{\partial v}{\partial t} + u \frac{\partial v}{\partial x} + v \frac{\partial v}{\partial y} + w \frac{\partial v}{\partial z} \right) = -\frac{\partial p}{\partial y} + \rho g_y + \mu \left(\frac{\partial^2 v}{\partial x^2} + \frac{\partial^2 v}{\partial y^2} + \frac{\partial^2 v}{\partial z^2} \right) \quad (2.2)$$

$$\rho \left(\frac{\partial w}{\partial t} + u \frac{\partial w}{\partial x} + v \frac{\partial w}{\partial y} + w \frac{\partial w}{\partial z} \right) = -\frac{\partial p}{\partial z} + \rho g_z + \mu \left(\frac{\partial^2 w}{\partial x^2} + \frac{\partial^2 w}{\partial y^2} + \frac{\partial^2 w}{\partial z^2} \right) \quad (2.3)$$

where: g gravity, p fluid pressure, μ dynamic viscosity and u , v and w are displacements. For practical applications special solutions of these Navier-Stokes differential equations were deduced, e.g.:

i. laminar flow between plates: $q = \frac{2a^3}{3\mu} \left(\frac{\partial p}{\partial x} \right)$ (2.4)

ii. laminar flow in circular tubes: $Q = \frac{\pi r^4}{8\mu} \left(\frac{\partial p}{\partial x} \right)$ (2.5)

iii. laminar Darcy flow: $v_i = \frac{k_{ij}}{\mu} \left(\frac{\partial p}{\partial x_j} \right)$ (2.6)

where q represents the flowrate and k_{ij} the permeability tensor.

The SI unit of permeability k is m^2 (also often used is Darcy (D): $1 \text{ D} = 1e-12 \text{ m}^2$). The hydraulic conductivity K (unit: m/s) is related to the permeability by the following relation:

$$K = \frac{\rho \cdot g \cdot k}{\mu} \quad (2.7)$$

The hydraulic gradient i is defined as follows:

$$i = \frac{dh}{dl} \quad (2.8)$$

where dh is the head loss and dl is the flow path length.

Tab. 2.1: Typical values of hydraulic conductivity for various rock and soil types (Domenico & Schwartz, 1990)

Type	Hydraulic Conductivity (m/s)
Unconsolidated Sedimentary Rocks	
Gravel	3×10^{-4} to 3×10^{-2}
Coarse sand	9×10^{-7} to 6×10^{-3}
Medium sand	9×10^{-7} to 5×10^{-4}
Fine sand	2×10^{-7} to 2×10^{-4}
Silt, loess	1×10^{-9} to 2×10^{-5}
Till	1×10^{-12} to 2×10^{-6}
Clay	1×10^{-11} to 4.7×10^{-9}
Non-weathered marine clay	8×10^{-13} to 2×10^{-9}
Sedimentary Rocks	
Karst and reef limestone	1×10^{-6} to 2×10^{-2}
Limestone, dolomite	1×10^{-9} to 6×10^{-6}
Sandstone	3×10^{-10} to 6×10^{-6}
Siltstone	1×10^{-11} to 1.4×10^{-8}
Salt	1×10^{-12} to 1×10^{-10}
Anhydrite	4×10^{-13} to 2×10^{-8}
Shale	1×10^{-13} to 2×10^{-9}
Crystalline Rocks	
Permeable basalt	4×10^{-7} to 2×10^{-2}
Fractured igneous and metamorphic rock	8×10^{-9} to 3×10^{-4}
Weathered granite	3.3×10^{-6} to 5.2×10^{-5}
Weathered gabbro	5.5×10^{-7} to 3.8×10^{-6}
Basalt	2×10^{-11} to 4.2×10^{-7}
Non-fractured igneous and metamorphic rock	3×10^{-14} to 2×10^{-10}

Tab. 2.1 shows typical values of hydraulic conductivity for various rocks and soil types. Permeability can be anisotropic and inhomogeneous as illustrated in Fig. 2.1 (in fact, permeability is a second rank tensor quantity).

The flow (seepage) velocity v is given by the product of the hydraulic gradient and the hydraulic conductivity:

$$v = K \cdot i \tag{2.9}$$

Depending on flow velocity and shape of low channels the flow can be either laminar or turbulent. According to Bear (1972), Darcy's law which assumes laminar flow is valid as long as the values of Reynolds number (Re) do not exceed the interval between 1 and 10 in case of porous media. The same holds for rock fractures (Zimmermann et al. 2004).

Reynold’s number is defined as follows:

$$Re = \frac{\rho \cdot v \cdot d}{\mu}, \quad (2.10)$$

where v is the specific flow discharge (unit: m/s) and d is the characteristic length of the medium (unit: m). According to Freeze & Cherry (1979) characteristic length of a porous medium can be taken as mean pore dimension, mean grain diameter, or some function of the square root of the permeability k as well as hydraulic fracture aperture.

In general, several flow regimes can be distinguished (note: given numbers are approximations only):

- | | |
|-------------------------------------|--------------------|
| ▪ viscous flow (Darcy) | $Re < 1$ |
| ▪ weak inertia flow | $1 < Re < 10$ |
| ▪ strong inertia flow (Forchheimer) | $10 < Re < 1000$ |
| ▪ transitional flow | $1000 < Re < 2300$ |
| ▪ turbulent flow | $Re > 2300$ |

The different flow regimes are characterized by different proportions of viscous and inertial forces.

High flow velocities (e.g. produced by large hydraulic gradients) and/or high Reynolds numbers can trigger onset of turbulent flow. The so-called Forchheimer equation can be used for this flow regime:

$$\frac{dp}{dl} = \frac{\mu \cdot v}{k} + \beta \cdot \rho \cdot v^2, \quad (2.11)$$

where β represents the Non-Darcy coefficient. If second term - which stands for inertial effects - in (2.11) is omitted, (2.11) becomes Darcy’s law. However, for flow in fractures under high normal stress the second term in (2.11) shows a v^3 -dependency (Ranjith & Darlington 2007). Fig. 2.2 illustrates how flow regime can change from linear to non-linear.

Fig. 2.1 illustrates a highly turbulent 3D fracture flow simulation with global $Re = 1e5$. Fig. 2.1 top shows the fracture width (opening) using the Hausdorff distance (Finenko & Konietzky, 2021), Fig. 2.1 middle shows local Re numbers, which cover several orders of magnitude up to about $1e6$. Fig. 2.1 bottom shows the streamlines superimposed on the aperture plot. Although the applied conditions are extreme, these figures illustrate the complexity of fluid flow in narrow and rough fractures.

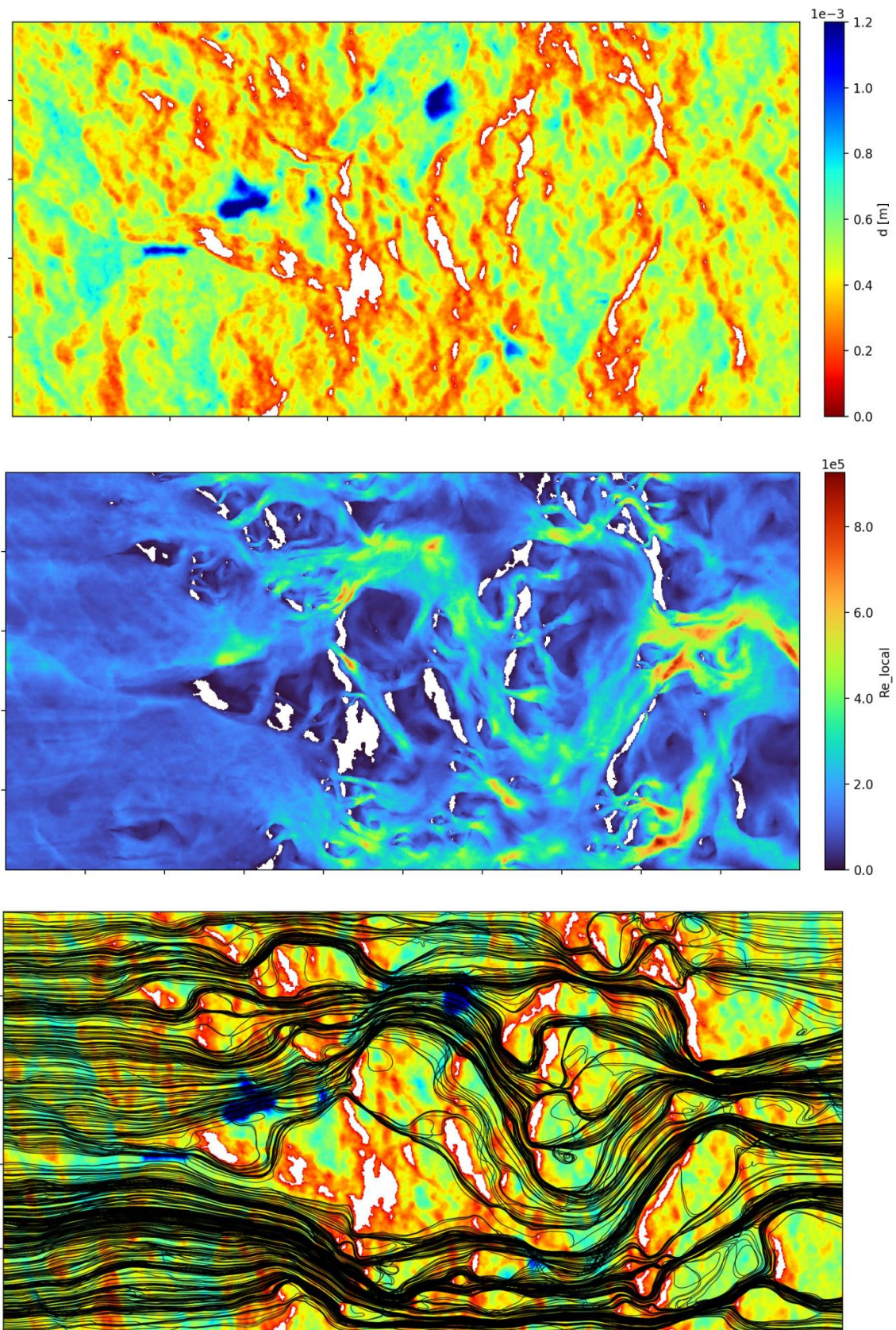


Fig. 2.1: Highly turbulent flow through a rough fracture, from top to bottom: fracture opening, local Re numbers and streamlines (Finenko & Konietzky, 2024b)

Finenko and Konietzky (2024a, 2024b) have investigated the flow through rough fractures via CFD simulations considering an extremely large range of Reynolds numbers from 1 up to 1E6 to cover the full spectrum from laminar to highly turbulent flow. Fig. 2.2 shows curve fitting between simulation results and the Forchheimer equation (2.11) by using only one data set for k and β . It becomes visible, that the fitting is not perfect. However, using two data sets for k and β a perfect fit can be obtained (see Fig. 2.3).

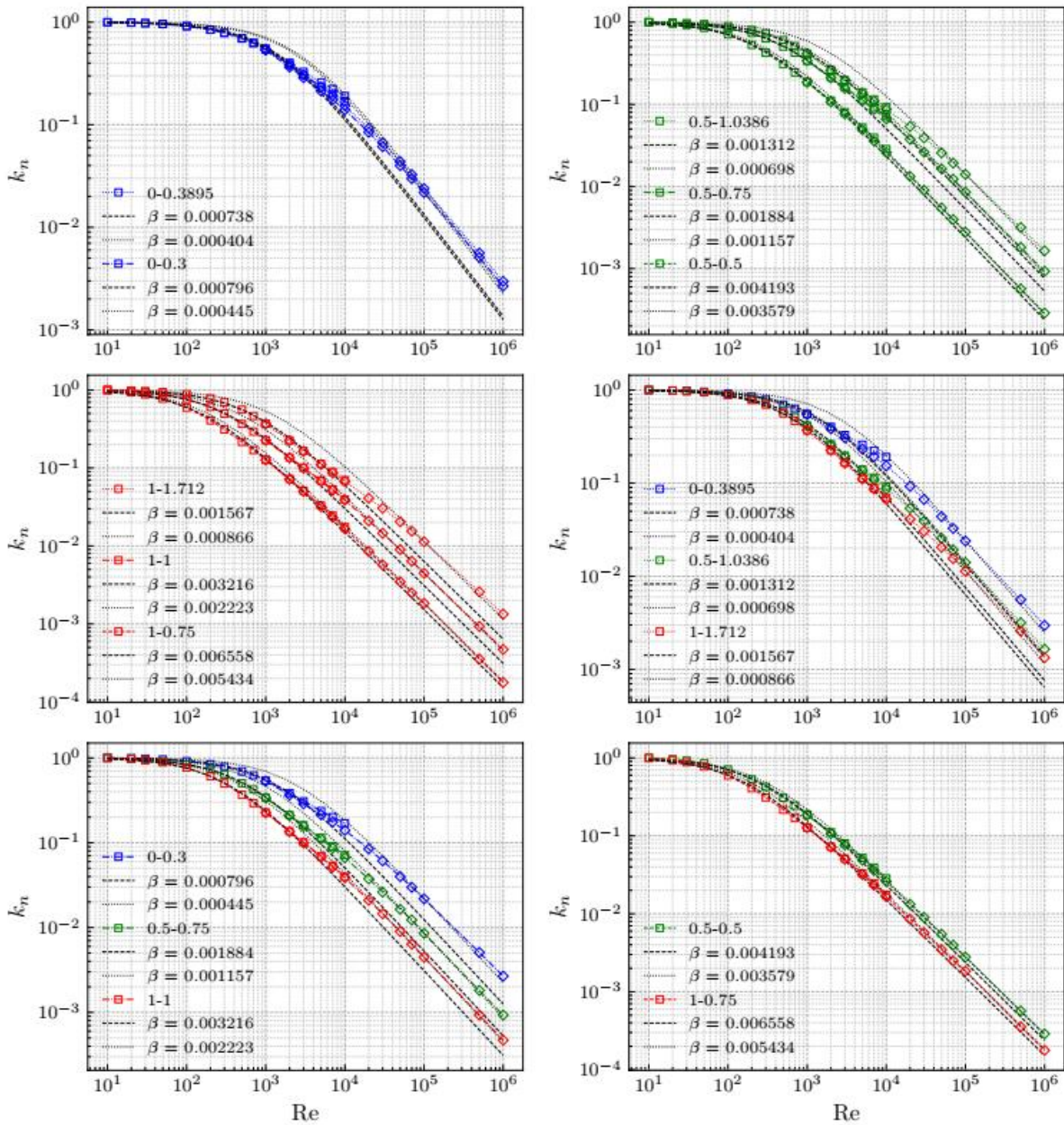


Fig. 2.2: Curve fitting of simulated flow through a fracture via the Forchheimer equation by using only one data set for parameters k and β (Finenko & Konietzky, 2024). The simulations cover different joint opening and shear displacement. k_n represents relative permeability.

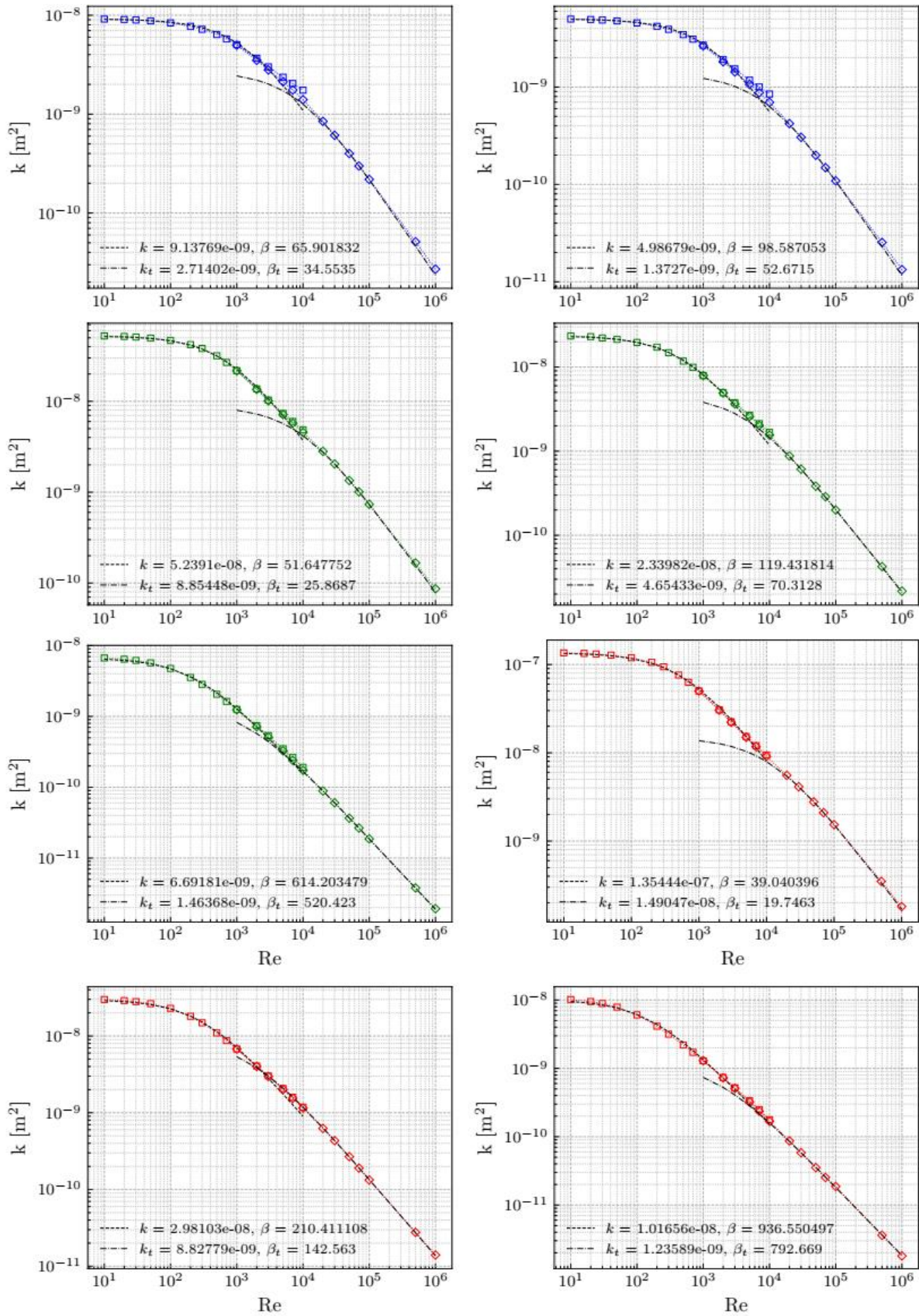


Fig. 2.3: Curve fitting of simulated flow through a fracture via the Forchheimer equation by using two data sets for parameters k and β (Finenko & Konietzky, 2024). The simulations cover different joint opening and shear displacement. k represents absolute permeability.

Another term often used in geohydraulics is transmissivity T_i (unit: m^2/s) of the i -th layer, which is the product of hydraulic conductivity multiplied with the layer or aquifer thickness d_i :

$$T_i = K_i \cdot d_i \tag{2.12}$$

Hydraulic diffusivity α_d (unit: m^2/s) is the ratio between transmissivity T and storativity S .

$$\alpha_d = \frac{T}{S} \tag{2.13a}$$

Another definition for hydraulic diffusivity is:

$$\alpha_d = \frac{K}{n\mu c} \tag{2.13b}$$

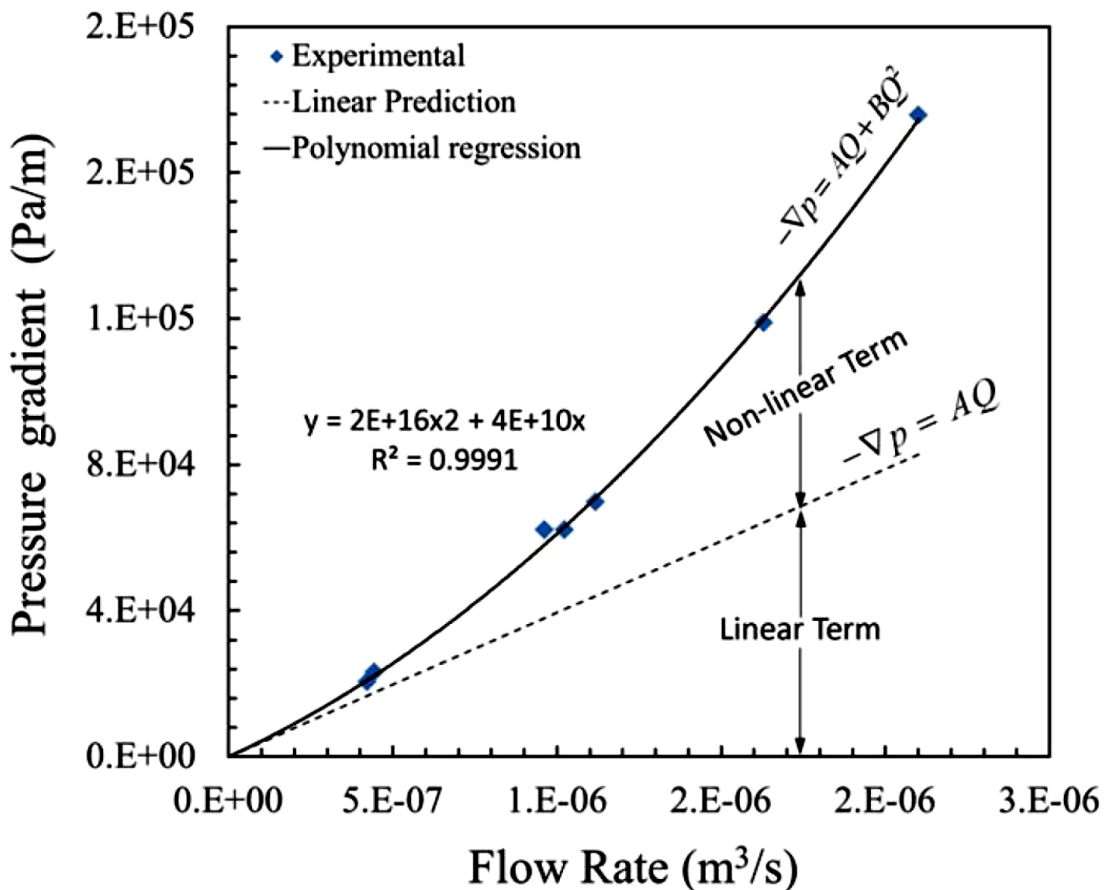


Fig. 2.4: Illustration of linear and non-linear flow rules (Javadi et al. 2014)

Where c (unit Pa^{-1}) is the total compressibility (= sum of compressibility of fluid and rock matrix). Compressibility is the inverse of the bulk modulus.

Storativity (dimensionless) defines the volume of water (V_w) which will be released during decrease of hydraulic head (h). The value is normalized by the aquifer area A .

$$S = \frac{1}{A} \cdot \frac{dV_w}{dh} \quad (2.14)$$

Porosity n describes the ratio of void volume V_v to total volume V :

$$n = \frac{V_v}{V} \quad (2.15)$$

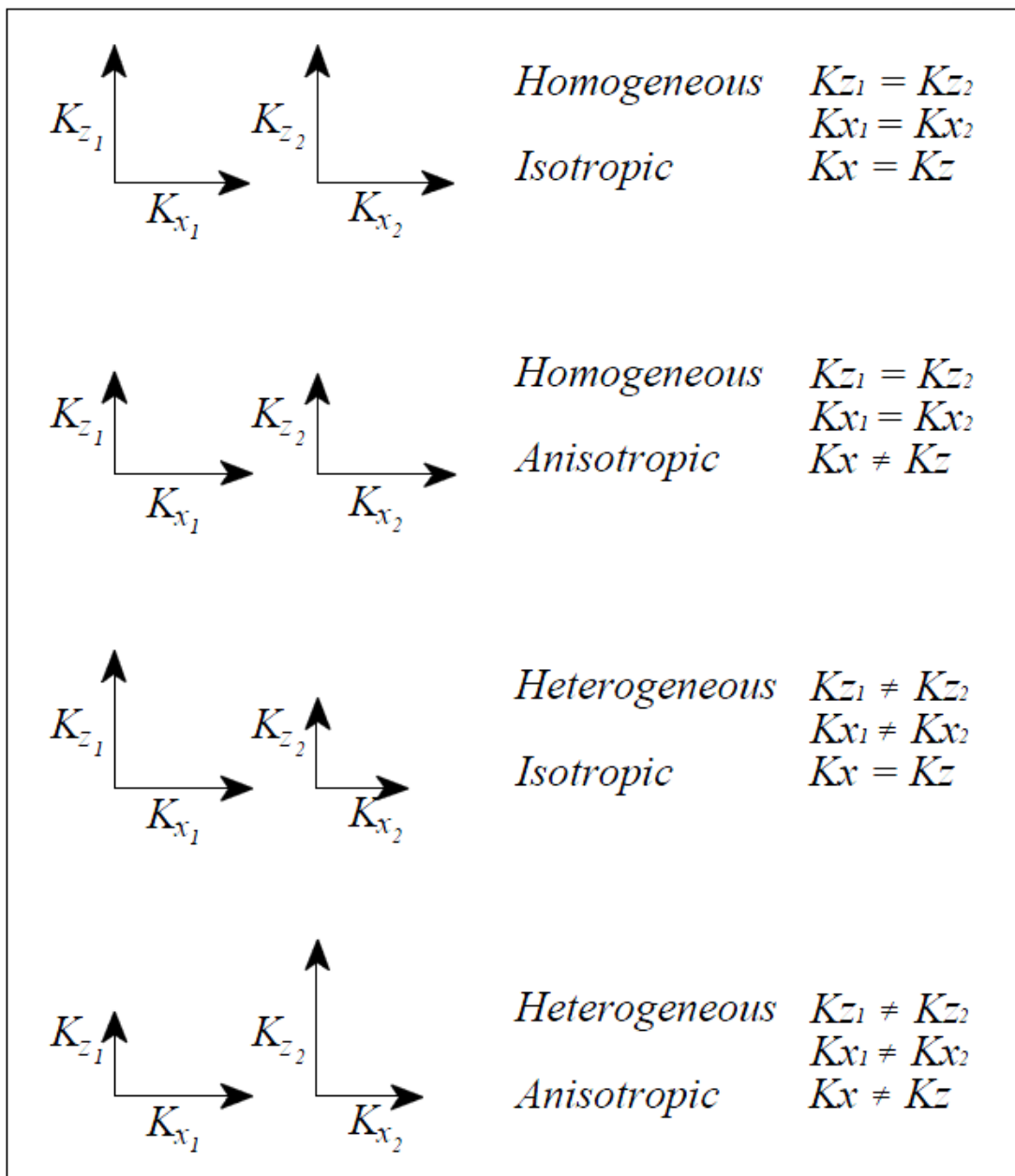


Fig. 2.5: Simple illustration of homogeneity, heterogeneity, isotropy and anisotropy of hydraulic conductivity (K) in a local (U.S. Army Corps of Engineers, 1999).

As an alternative to porosity the term void ratio e defined as the ratio between void volume V_v and solid volume V_s is often used:

$$e = \frac{V_v}{V_s} \quad (2.16)$$

Porosity and void ratio can be converted as follows:

$$e = \frac{n}{1-n} \quad n = \frac{e}{1+e} \quad (2.17)$$

Porosity of loose soils or sediments can reach up to about 70 %, sedimentary and some igneous rocks have porosities between about 10 % and 50 %, magmatic and metamorphic rocks have porosities between about 0.1 % and 5 %. Please note, that we have to distinguish between total, open and closed porosity (total porosity = open porosity + closed porosity).

The compressibility of the fluid is governed by the corresponding bulk modulus K_F :

$$K_F = \frac{\sigma_{iso}}{\varepsilon_v} \quad (2.18)$$

where σ_{iso} means isotropic stress and ε_v volumetric deformation. The compressibility of fluids is temperature dependent. Pure water at room temperature has a bulk modulus of about 2 GPa and can be assumed as incompressible for many (but not all!) applications. If gases are resolved in water the bulk modulus can be significantly reduced. In case of gases the 'ideal gas law' is valid:

$$p \cdot V_{spec} = R \cdot T \quad (2.19)$$

where p is the gas pressure, V_{spec} is the specific volume, R is the specific gas constant and T the absolute temperature.

Under isothermal conditions the following fundamental equation holds:

$$p \cdot V_{spec} = \text{const.} \quad (2.20)$$

Another form of the 'ideal gas law' is:

$$\frac{p}{\rho} = R \cdot T \quad (2.21)$$

Real gases, especially under high pressure, show some deviations from the 'ideal gas law'. Therefore, a 'gas deviation factor' f_G is introduced to take this into account:

$$\frac{p}{\rho} = f_G \cdot R \cdot T \quad (2.22)$$

It should be noticed, that the Navier-Stokes equations and the deviated special cases are based on the assumption, that fluid flow at the boundaries is zero. This assumption is approximately true for most (but not all!) geotechnical applications. If this assumption

is violated the flow is called ‘Knudson’ or ‘slip’ flow. This leads to an apparent permeability K_{app} which is related to the ‘true’ permeability by considering the so-called ‘Klinkenberg’ effect.

$$K_{app} = K \left[1 + \frac{4\sqrt{n} \cdot T \cdot B}{5\sqrt{2}\pi \cdot \sqrt{K} \cdot d_M^2 \cdot p} \right] \tag{2.23}$$

Where B is the Boltzmann constant and d_M the effective molecular diameter. The above given equation can be simplified by the following expression:

$$K_{app} = K \left[1 + \frac{p^c}{p} \right] \tag{2.24}$$

where p^c is called ‘characteristic pressure’. If $p > 10p^c$ the Klinkenberg effect can be neglected, otherwise a correction has to be made. This is often the case in lab tests with gases. The Klinkenberg corrected permeability can be computed from the straight line intercept on a plot of measured permeability against inverse mean pressure as shown in Fig. 2.6. Fig. 2.7 illustrates the difference between steady-state and unsteady-state test conditions using rock samples.

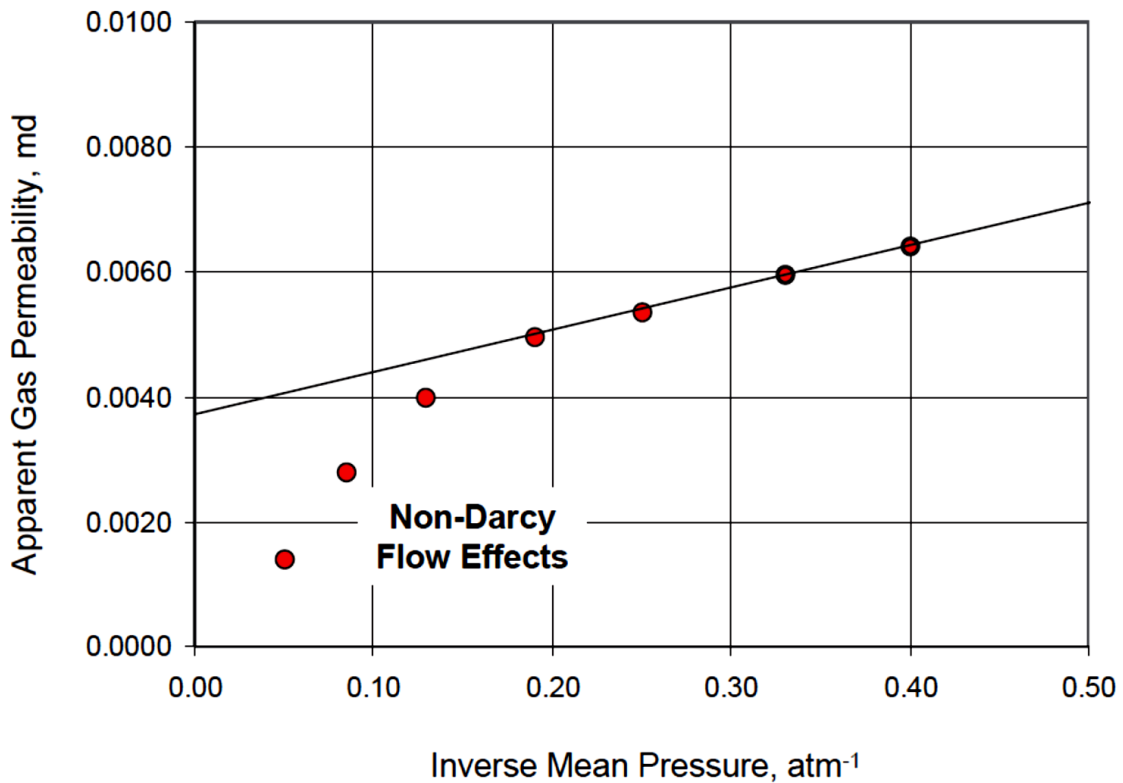


Fig. 2.6: Klinkenberg plot showing the correction procedure (Rushing et al., 2004).

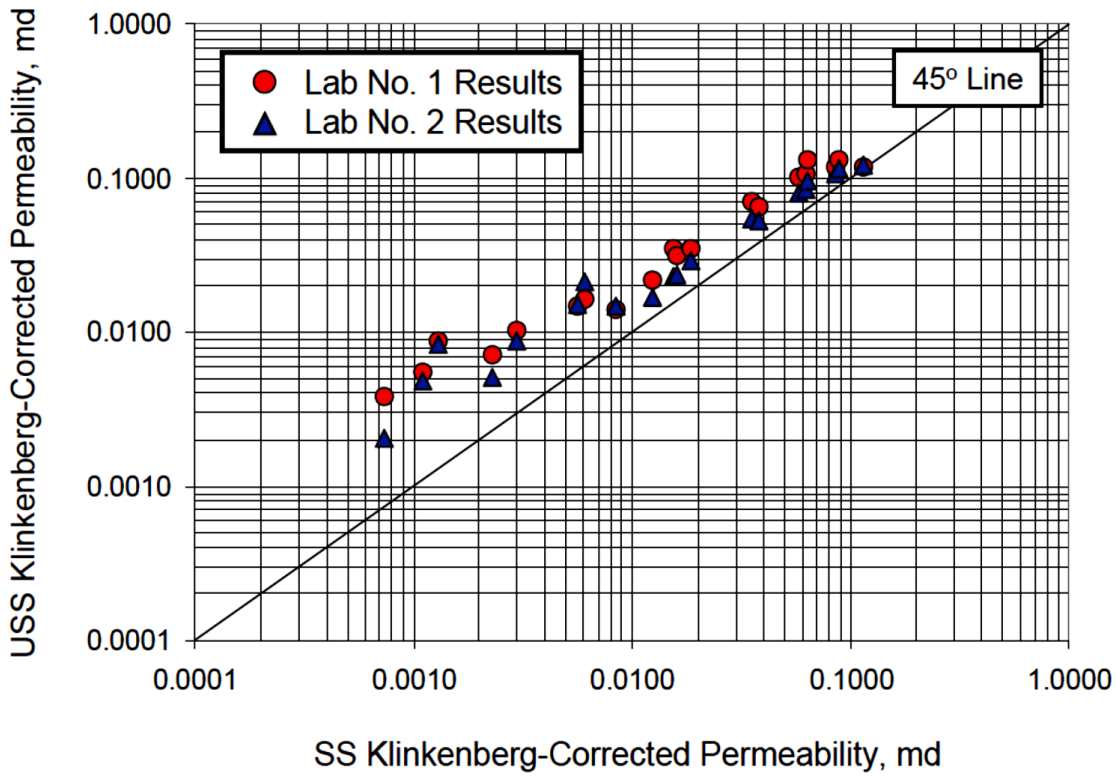


Fig. 2.7: Comparison of lab test results for Klinkenberg corrected permeabilities using steady-state and unsteady-state lab test conditions (Rushing et al., 2004).

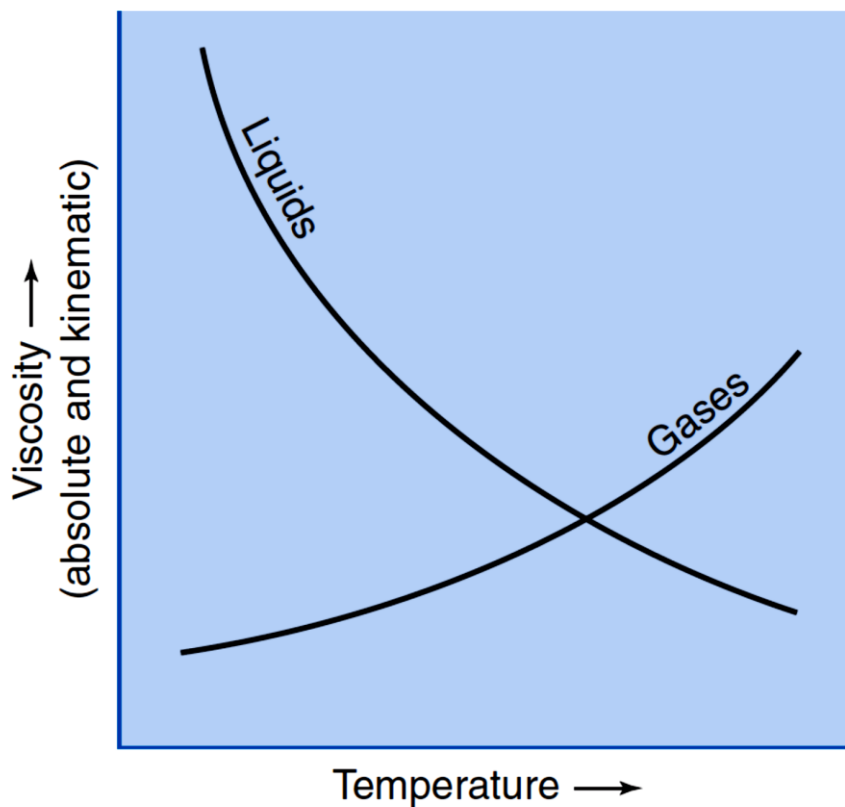


Fig. 2.8: General behaviour of temperature dependent viscosity for gases and liquids

Tab. 2.2: Typical values for viscosity of different materials

Material	Typical dynamic viscosity at room temperature / Pa·s
Granite	1e19
Olive oil	0.08
Motor oil	0.1
Water	9e-4
Honey	5
Blood	3e-3
Air	18e-6
Carbon dioxide	15e-6
Mercury	1.5e-3

Absolut viscosity, also called dynamic viscosity η (unit: Pa·s), can be defined as follows (note, that viscosity and density are temperature dependent, like shown in Fig. 2.6 and 2.9):

$$\eta = G \cdot t \tag{2.25}$$

where G means the shear modulus and t the time.

Kinematic viscosity ν (unit: m²/s) is defined as quotient between dynamic viscosity and density:

$$\nu = \frac{\mu}{\rho} \tag{2.26}$$

According to the viscosity the fluids can be classified (Fig. 2.10). The ideal fluid (in first approximation valid for water) cannot transmit shear stresses. For Newtonian fluids the shear stress is linear proportional to the shear deformation. For Non-Newtonian fluids a non-linear relation between shear stress and shear strain is valid.

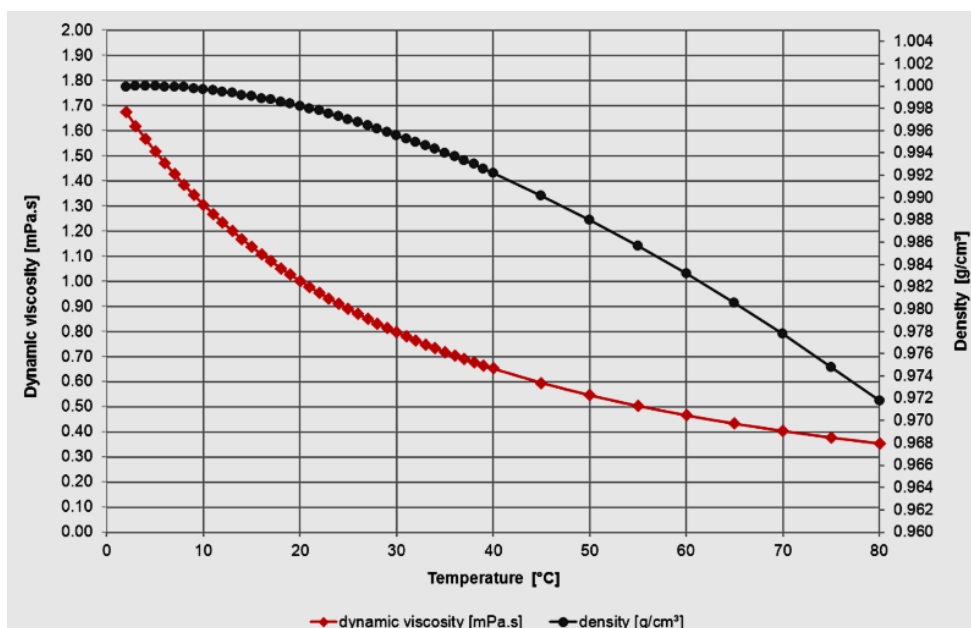


Fig. 2.9: Water viscosity and density versus temperature (www.viscopedia.com)

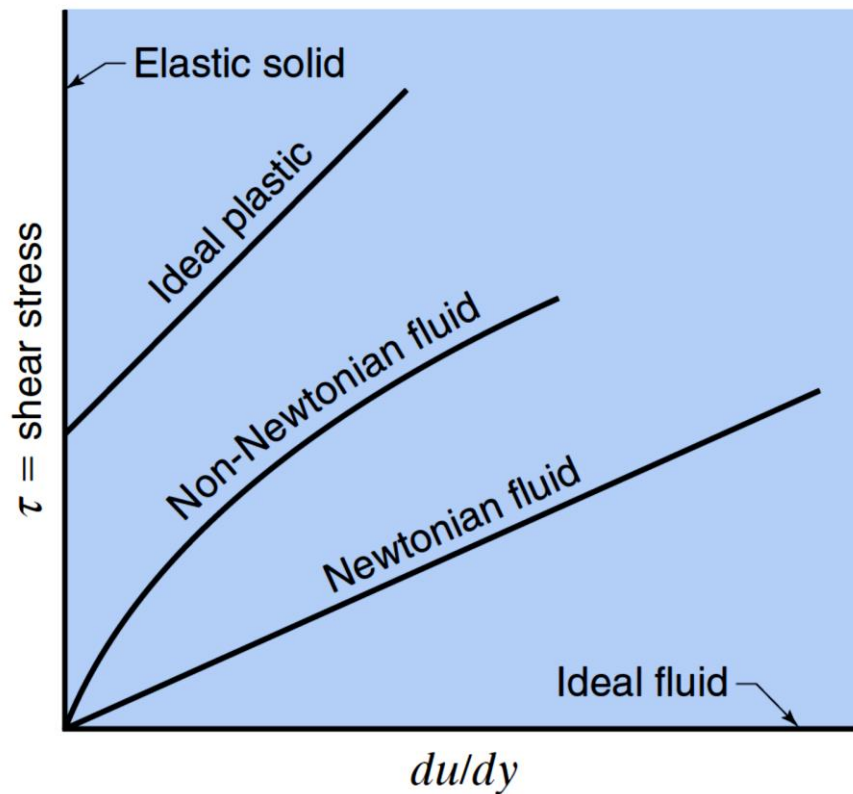


Fig. 2.10: Classification of fluids according to their viscosity (shear stress vs. shear strain)

3 Flow in fractured rock masses

Assuming an impermeable rock matrix, flow occurs only along joints and the so-called ‘cubic law’ (Eq. 2.4) can be applied. If fracture sets exist, an equivalent permeability can be given, e.g. for joints parallel to the *i*-direction:

$$k_i = \frac{\rho_w \cdot g \cdot a^3}{12 \cdot \mu \cdot S_i} \quad (3.1)$$

where: *a*: joint aperture, *g*: gravity, ρ_w : density of water, μ : dynamic viscosity, *S_i*: spacing between joints.

Besides equivalent permeability flow through fractures can be simulated in an explicit manner, for instance using the Discrete Element Method (DEM) or the Extended Finite Element Method (XFEM). A detailed analysis of the flow through a fracture with high resolution can be performed via Continuum Fluid Mechanics (CFD) codes. Exemplary, Fig. 3.1 illustrates the flow regime inside a fracture using streamlines and flow vectors. Example in Fig. 3.1 shows laminar and local turbulent flow regime.

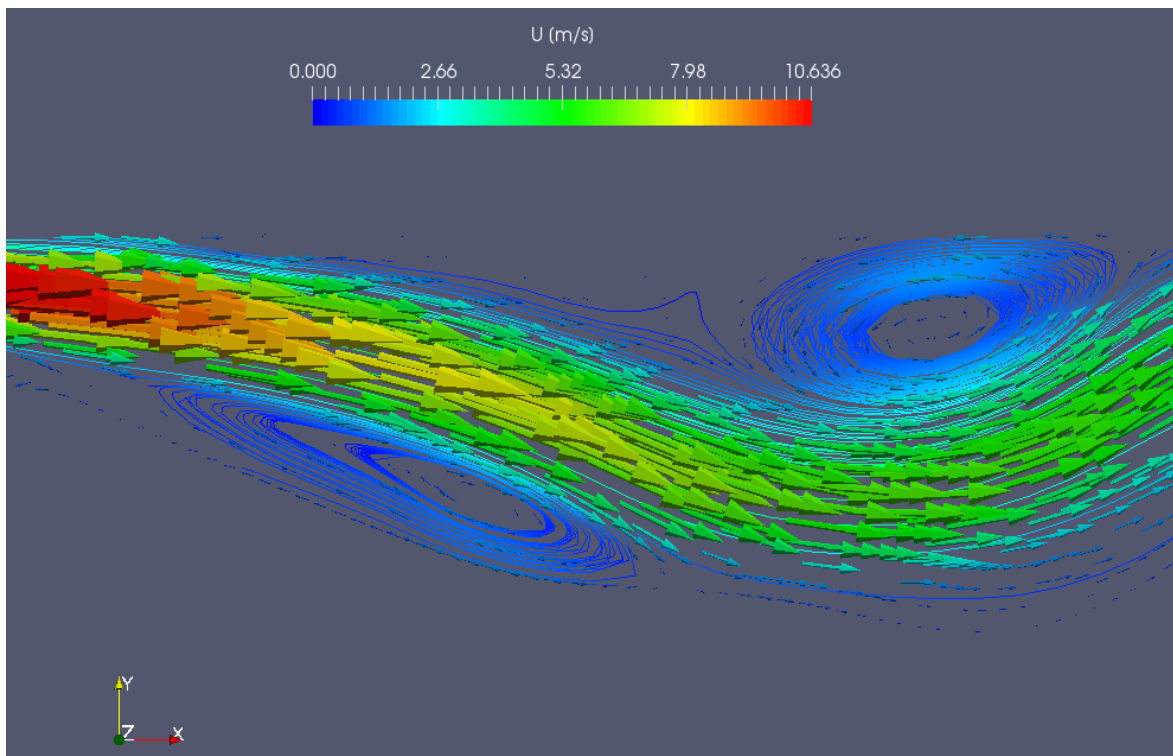
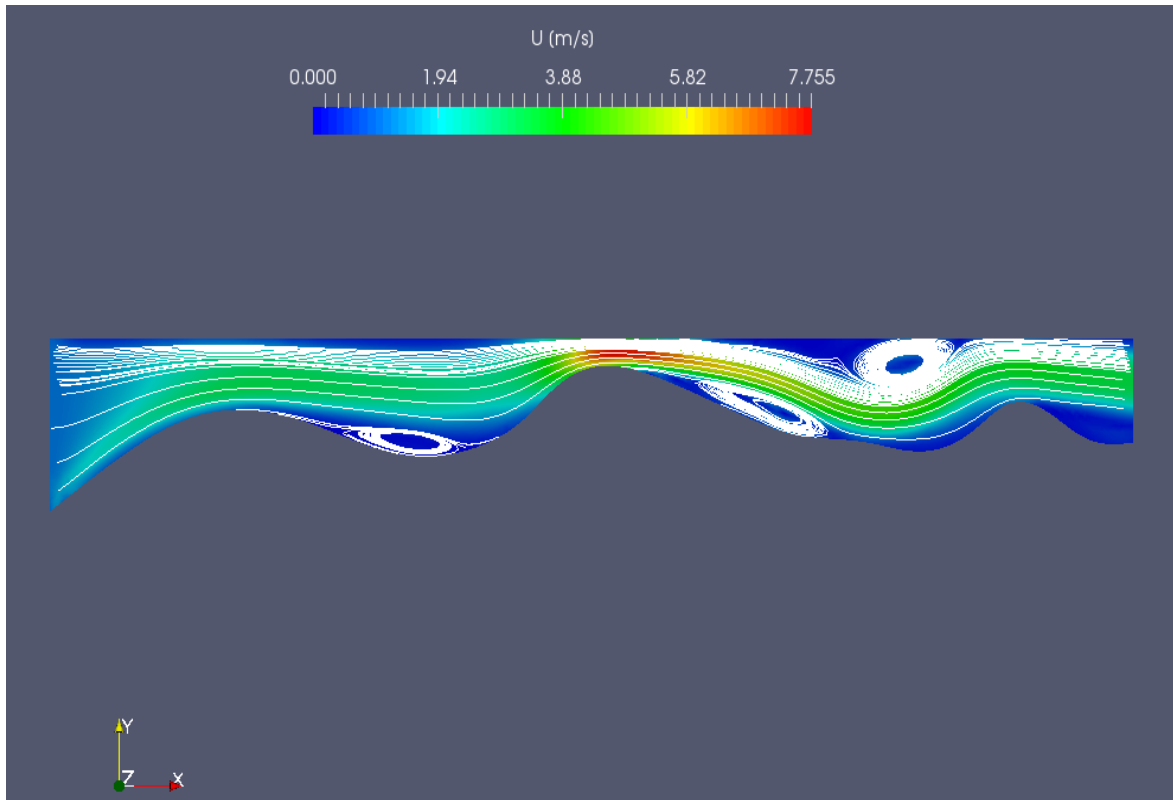


Fig. 3.1: Dominant laminar flow through a fracture with local turbulences: top: complete model, bottom: detailed plot [Finenko & Konietzky, 2018]

Fig. 3.2 shows typical values for seepage and deduced permeability using the simple formula of flow through parallel plates (see Eq. 3.1). The data given in Fig. 3.2 assume constant joint opening, laminar flow and constant spacing as explained in Fig. 3.2. The rock matrix is assumed to be impermeable, that means water flow occurs only along

the joints. Porosity and permeability are highly stress dependent like document by Fig. 3.3. Due to higher stresses at greater depths fractures becomes closed and/or crack development is limited.

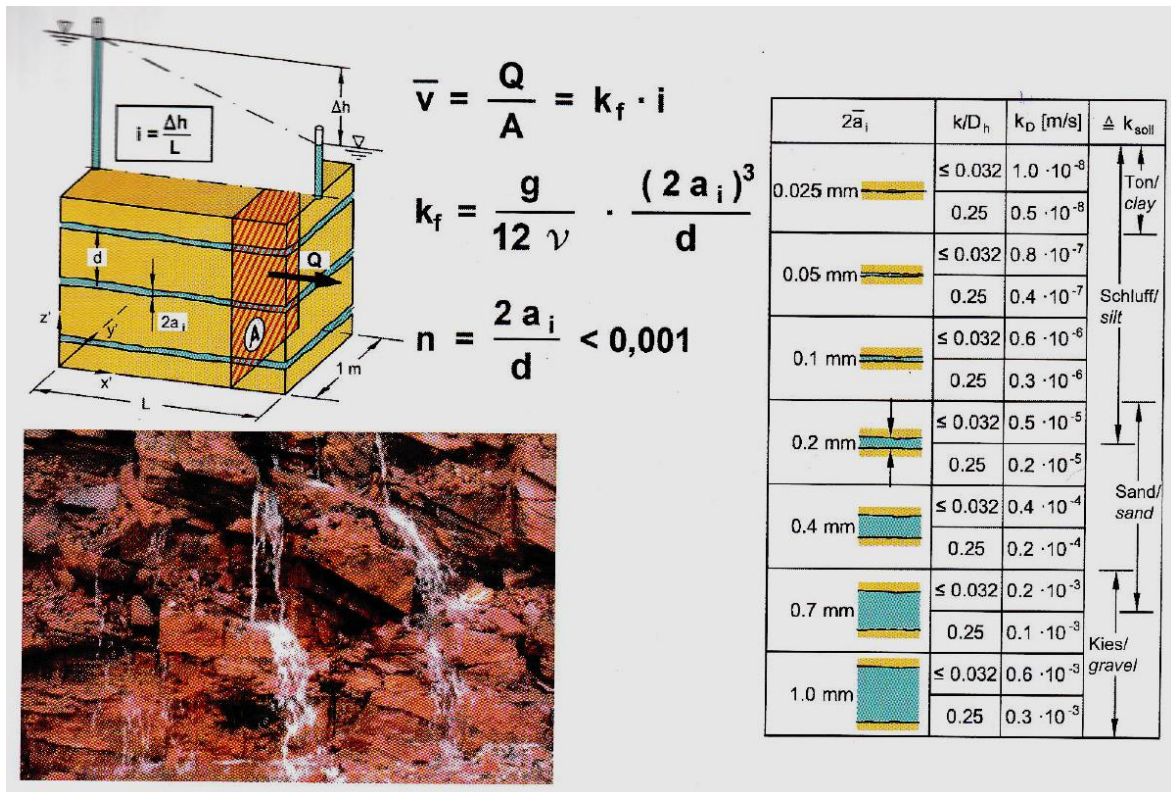


Fig. 3.2: Seepage flow through joints and equivalent permeability in comparison with soils [Wittke et al., 2021]

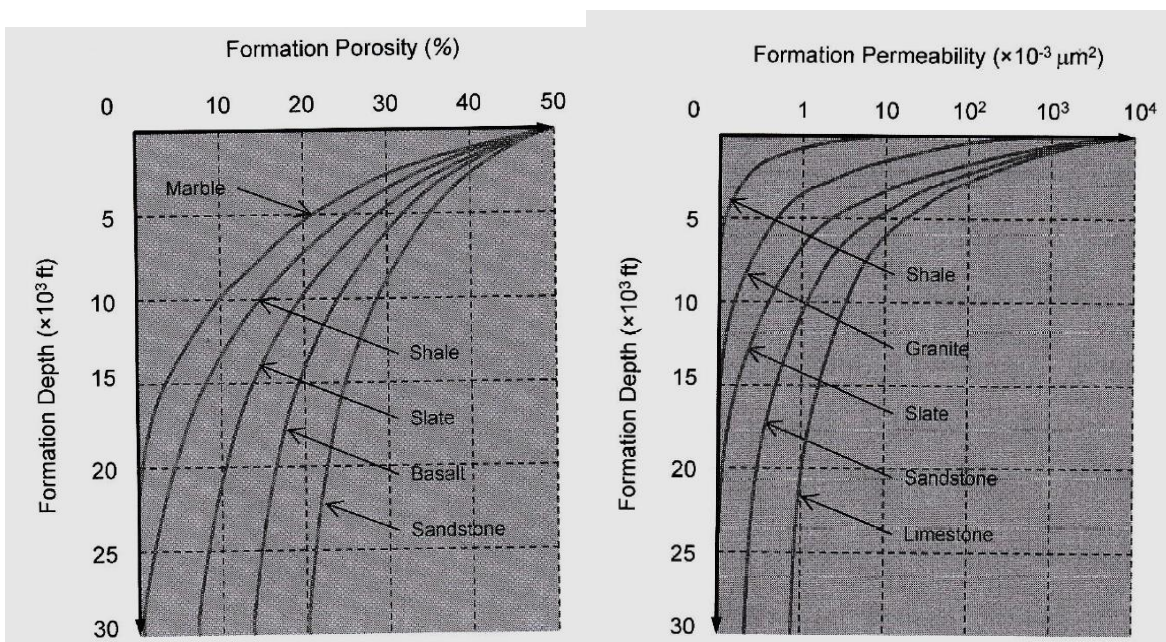


Fig. 3.3: Porosity and permeability of rocks as function of depth [Aadnoy & Looyeh, 2011]

Achtziger-Zupancic et al. (2017) have compiled 29.000 in-situ permeabilities of crystalline rocks to deduce general trends for the relation between permeability and depth. Considering all data the deduced the following relation (k in m^2 and z in km):

$$\log(k) = -1.5 \cdot \log(z) - 16.3 \quad (3.2)$$

Fig. 3.4 illustrates all the data and the general trend, whereas Fig. 3.5 shows subsets for different geological (tectonic) regions.

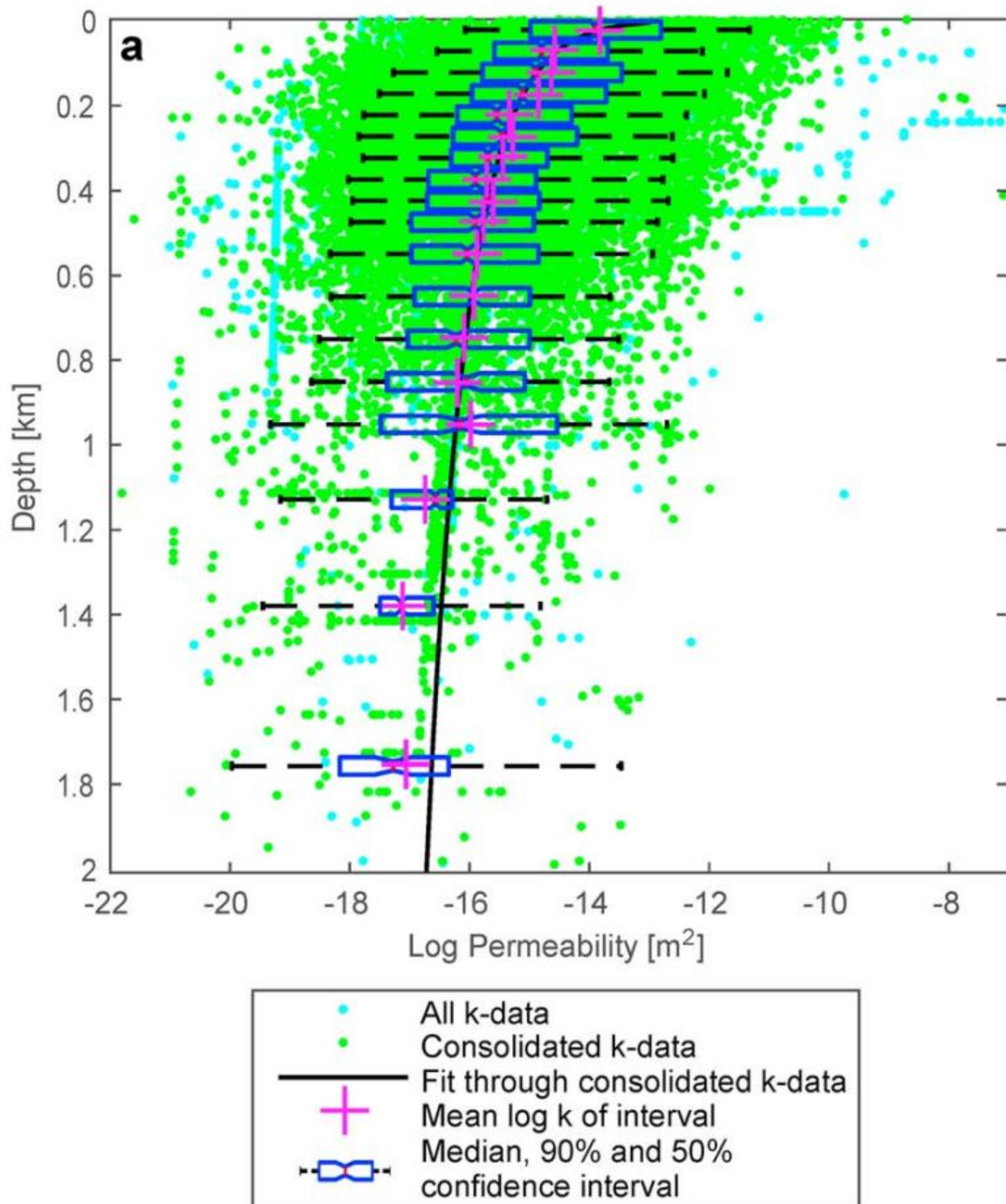


Fig. 3.4: Permeability vs. depth based on world-wide data sets [Achtziger-Zupancic et al., 2017]

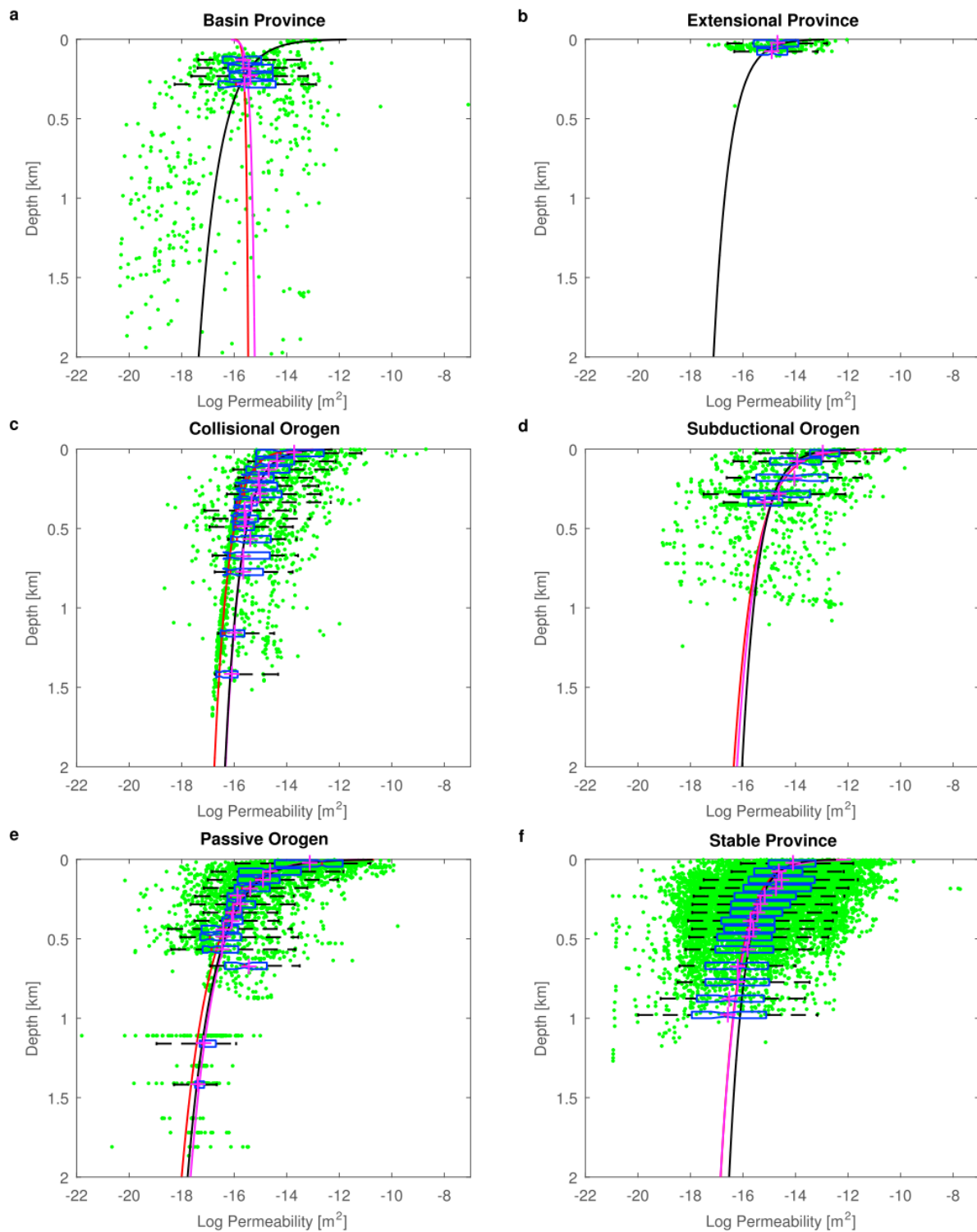


Fig. 3.5: Sub-data set for permeability (green) vs depth and its regression (black, solid line), the mean log k (pink crosses) and the median log k (red center of the boxplot) with 50% (blue) and 90% (black, dashed line) confidence interval at each depth for the geological provinces. The red and the pink solid curves describe the regression through the log median and the log mean permeability, respectively. [Achtziger-Zupancic et al., 2017]

4 Gas flow in geomaterials

For unsaturated low porosity soils and rocks gas flow might be an important process. Such processes are relevant for instance in coal or shale gas deposits, radioactive waste repositories or for CO₂ sequestration. As long as dominant flow channels do not exist, Fick’s first law can be applied to describe the gas flow by a diffusion process:

$$q_i = -D \frac{\partial C}{\partial x_i} \tag{4.1}$$

where q is the mass transfer rate, D is the diffusion coefficient and C is the concentration. In general D is a tensor value (D_{ij}) and can therefore have different values for different directions. First Fick’s law applies for stationary conditions, whereas the second Fick’s law considers instationary processes.

$$\frac{\partial C}{\partial t} = D \left(\frac{\partial^2 C}{\partial x^2} + \frac{\partial^2 C}{\partial y^2} + \frac{\partial^2 C}{\partial z^2} \right) \tag{4.2}$$

Fig. 4.1 and 4.2 illustrate Fick’s diffusion laws.

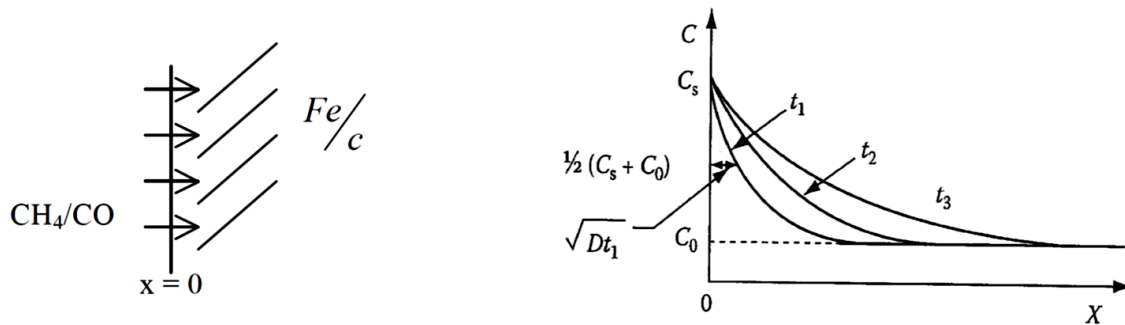


Fig. 4.1: Illustration of first Fick’s law (Utah, 2020)

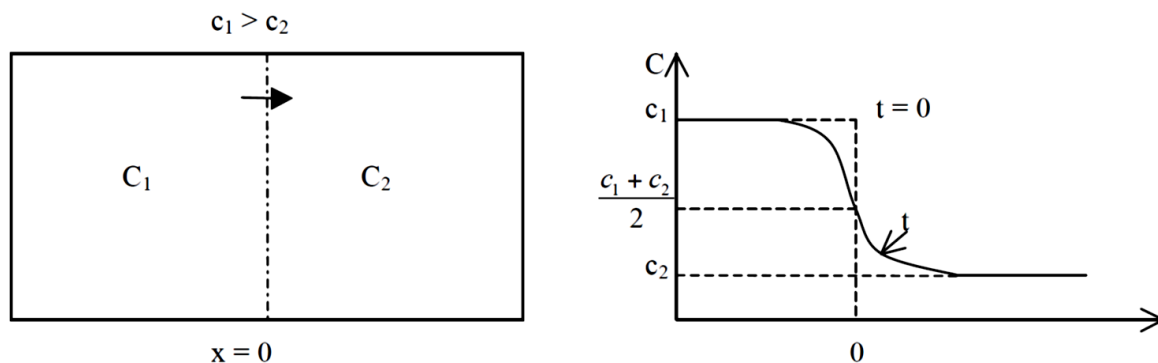


Fig. 4.2: Illustration of second Fick’s law (Utah, 2020)

Exemplary, Fig. 4.3 shows the evolution of NaCl above a sandstone core plug as function of time. Curve shape is controlled by the diffusivity, which is represented in Fig. 4.3 by the relative diffusivity number F .

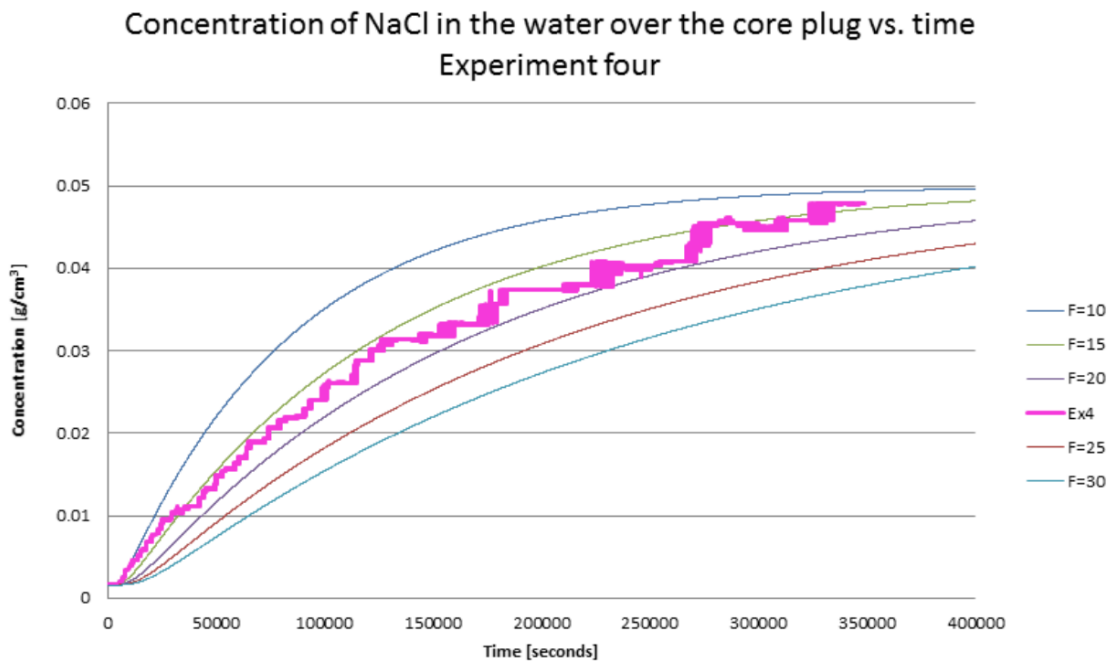


Fig. 4.3: Concentration of NaCl in water over a sandstone core plug versus time: experimental data (Ex4) and curves according to Fick's first law (F = relative diffusivity) (Blytt, 2017)

Exemplary, Fig. 4.4 shows a set of typical curves obtained by Fick's second law for gas diffusion in a concrete structure as function of depth and time. The underlying diffusion coefficient was obtained by lab testing.

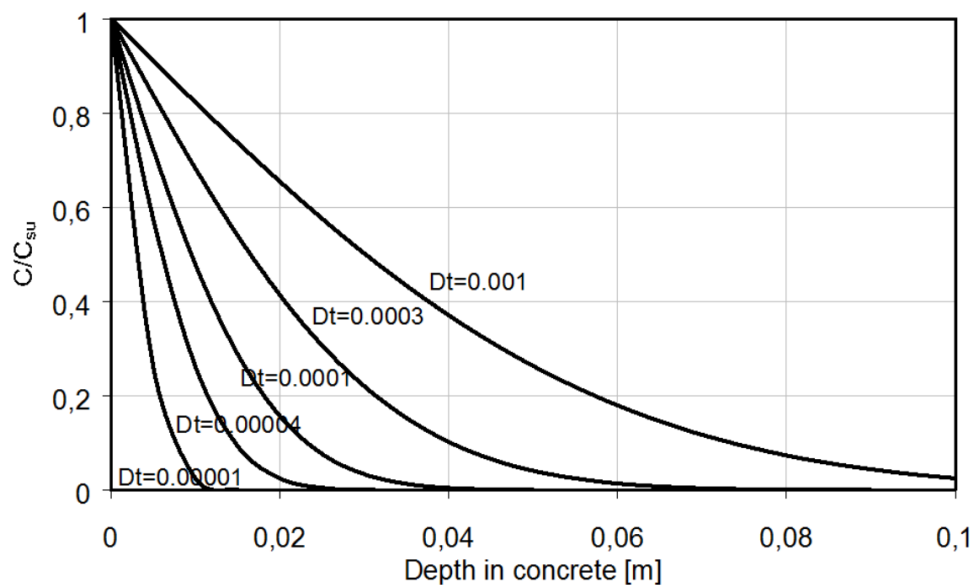


Fig. 4.4: Volatile organic compound relative concentration in concrete as function of depth and time according to second Fick's law (Sjoberg et al., 2010)

5 Hydro-mechanical coupling

The components of hydro-thermo-mechanical (HTM) coupling are illustrated in Fig. 5.1. The coupling always acts in both directions (two-way-coupling). Nevertheless, depending on the specific situation certain coupling may be dominating in respect to considered task. This chapter concentrates only on one aspect of hydro-mechanical (HM) coupling: the effective stress concept.

Effective stresses govern the deformation and failure pattern. These effective stresses are given by the following equation:

$$\sigma_{ij}^{eff} = \sigma_{ij}^{tot} - \delta_{ij} \cdot pp \cdot \alpha \tag{5.1}$$

where σ_{ij}^{eff} is the effective stress, σ_{ij}^{tot} is the total stress, pp is the pore or joint water pressure and α is the Biot coefficient. The Biot coefficient is defined as follows:

$$\alpha = 1 - \frac{K_S}{K_G} \tag{5.2}$$

with the drained (dry) bulk modulus K_S and the bulk modulus of grains K_G . Another often used term is the Biot modulus M_B (K_w is the fluid bulk modulus):

$$M_B = \frac{K_w}{n + (\alpha - n)(1 - \alpha) \cdot \frac{K_w}{K_S}} \tag{5.3}$$

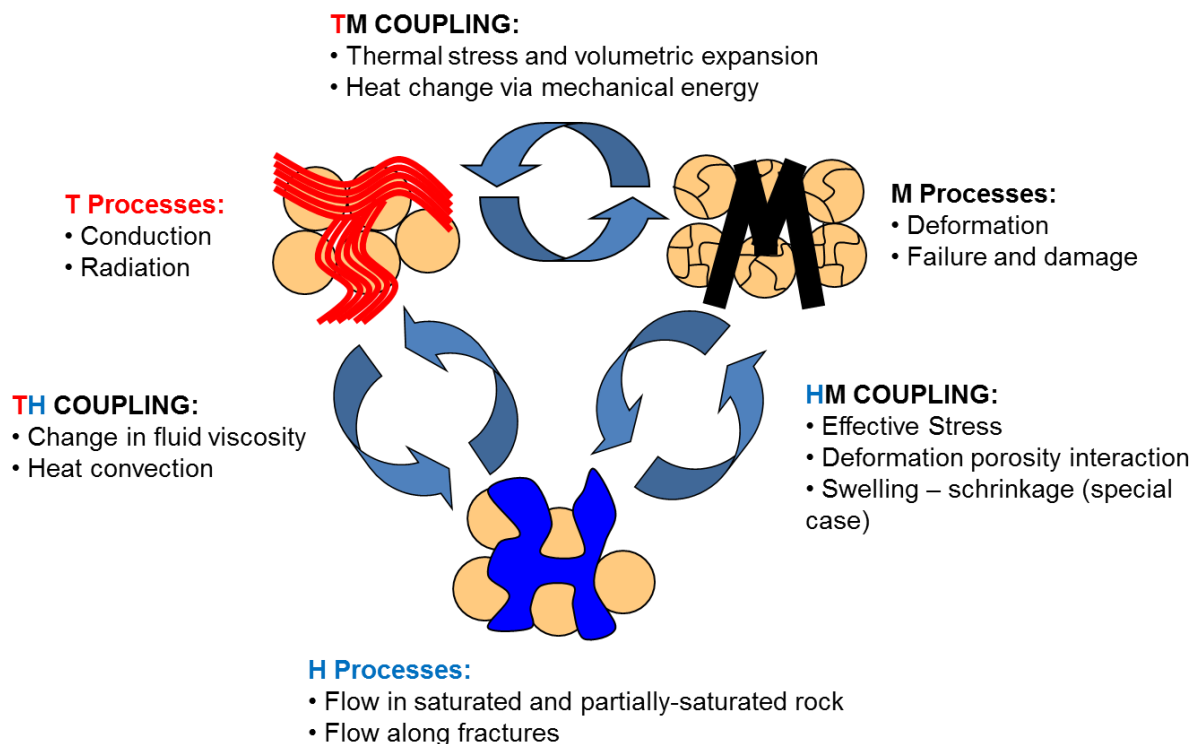


Fig. 5.1: General illustration of elements of HTM-coupling in geotechnics

For soils α is set to zero in most cases, for intact rocks α varies between 0 and 1 (typical value is 0.6). However, for rocks at failure α will also reach 1, at least locally. With ongoing damage inside the rock the Biot coefficient will increase (Tan, Konietzky & Frühwirth, 2015). Increasing damage causes increasing permeability (see Fig. 5.2). Also, the Biot coefficient can be anisotropic depending on the microstructure of the rock (Tan & Konietzky, 2014b).

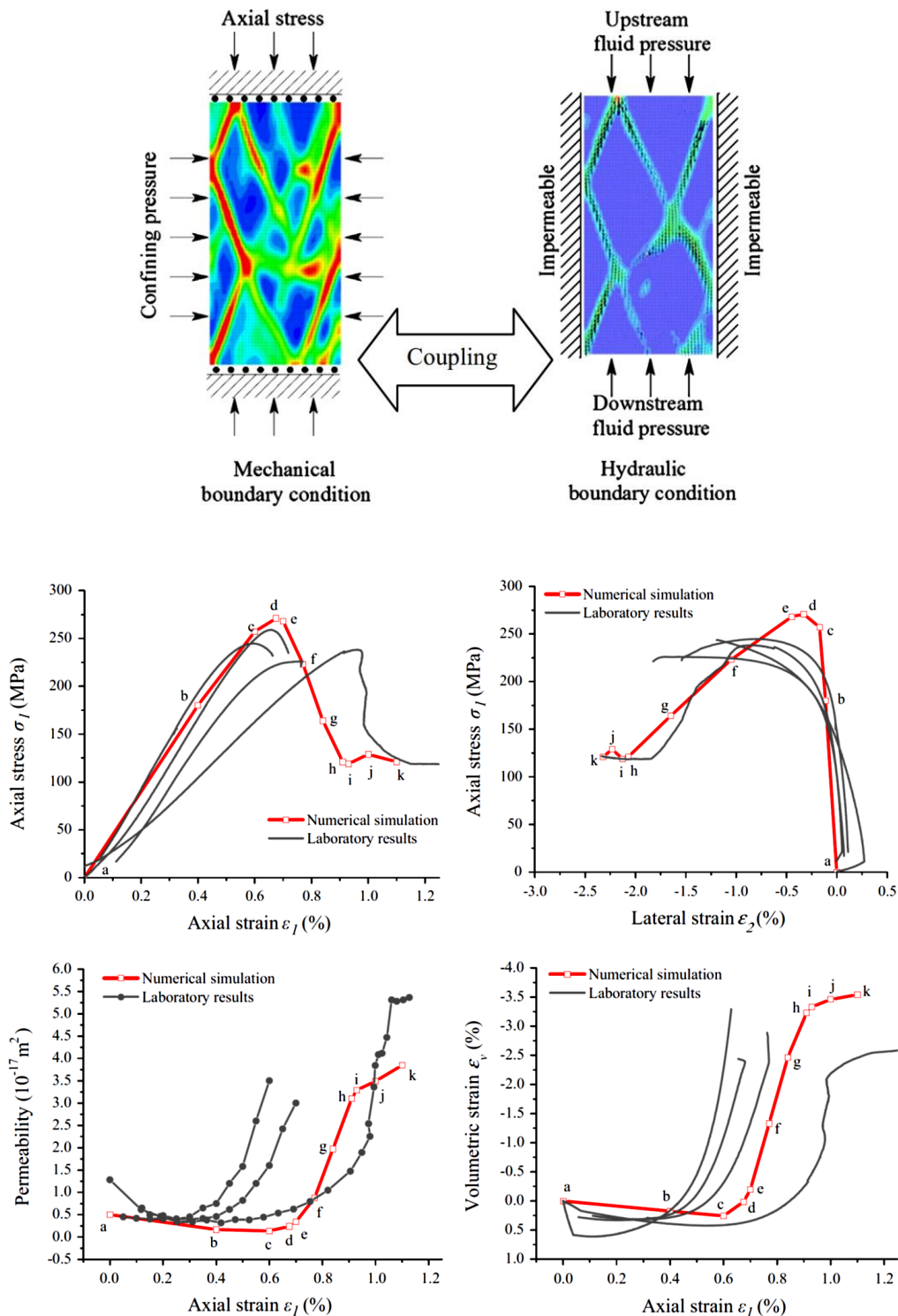


Fig. 5.2: Hydro-mechanical coupled behaviour of rock sample under 3-axial compression (Tan, Konietzky & Frühwirth, 2014a)

Fig. 5.3 illustrates the influence of porosity and pore shape on the Biot-coefficient incl. its anisotropy.

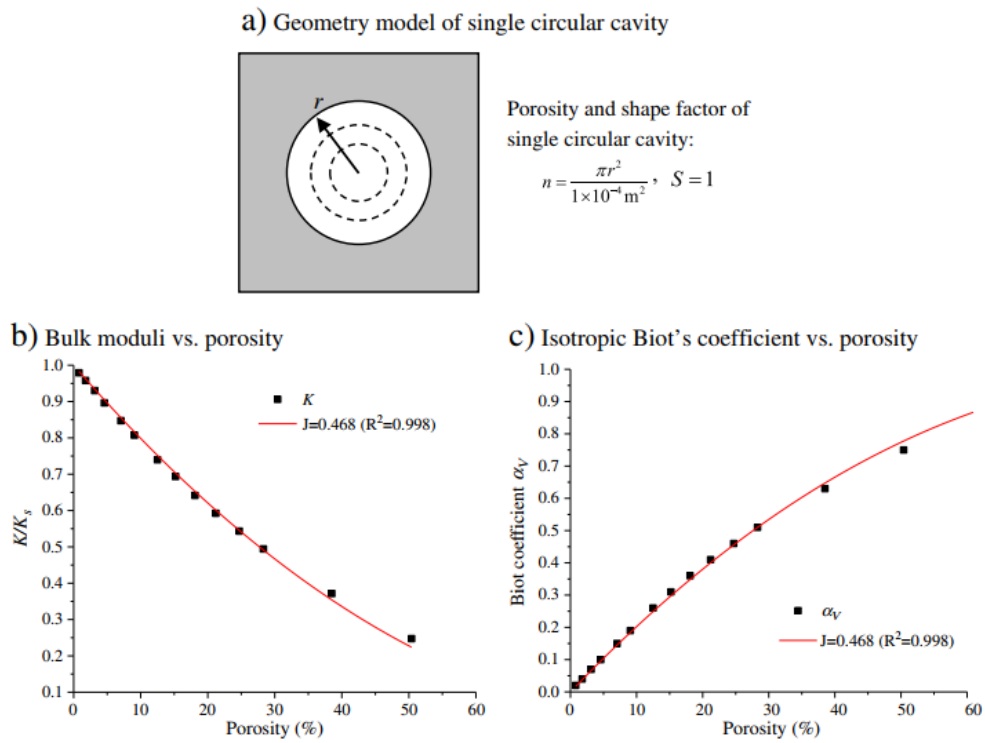


Fig. 8. Relation between poroelasticity parameters and cavity size (circular).

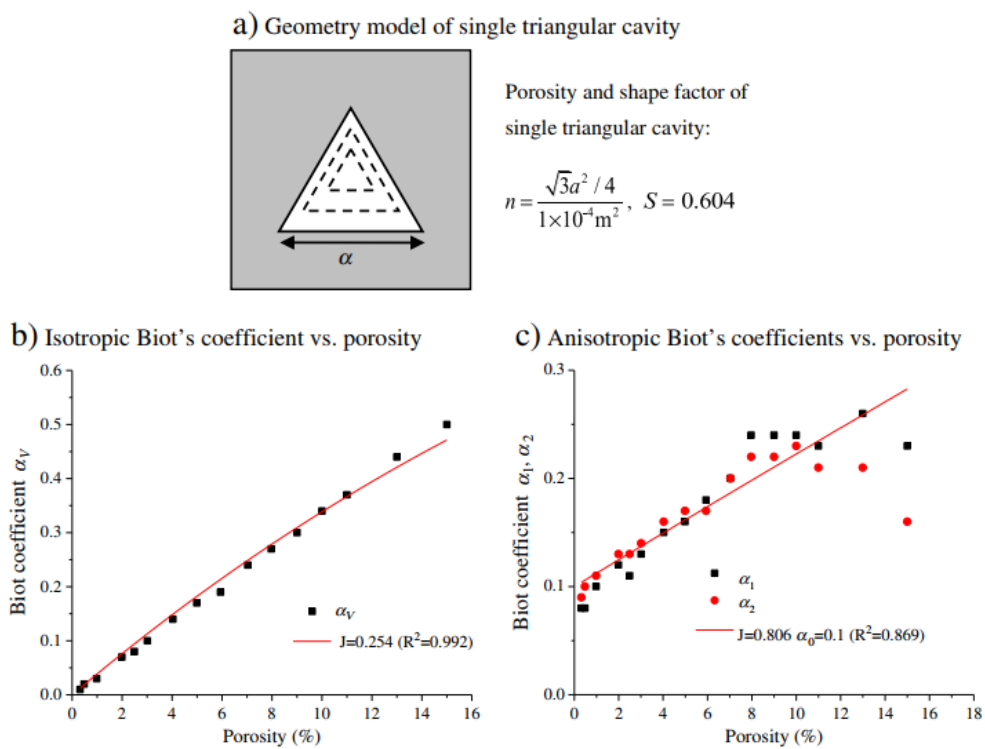
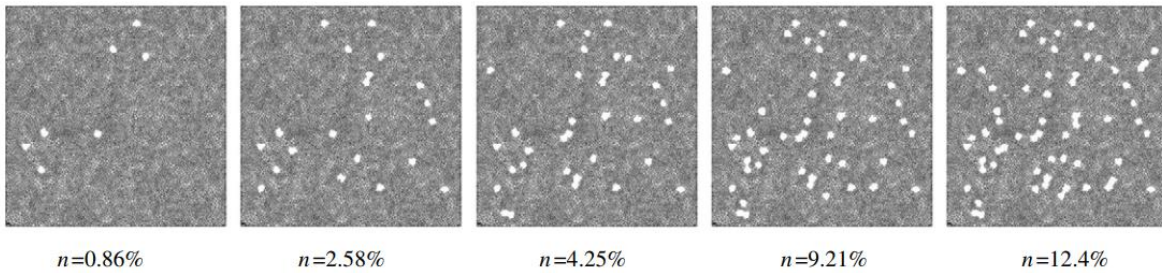
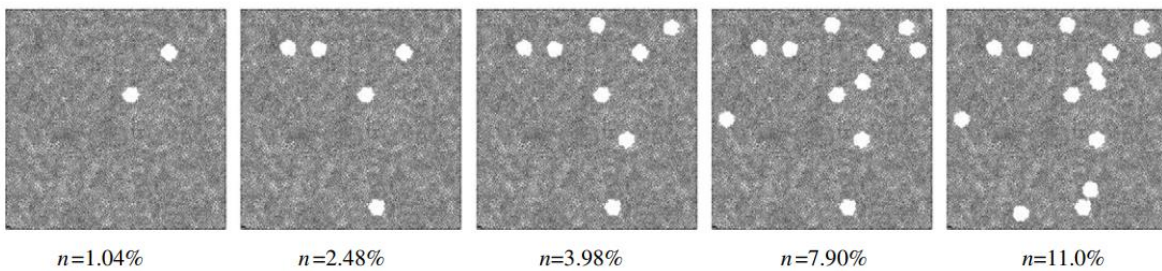


Fig. 5.3: Influence of porosity on Biot-coefficient incl. its anisotropy (Tan & Konietzky, 2014b)

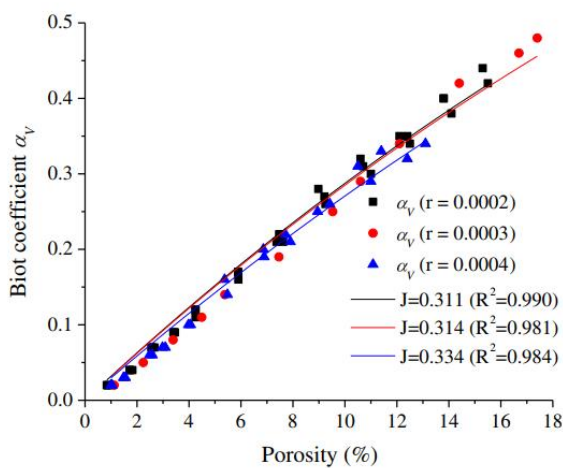
Fig. 5.4 shows simulations results for the Biot-coefficient assuming randomly distributed circular pores which create different porosities.



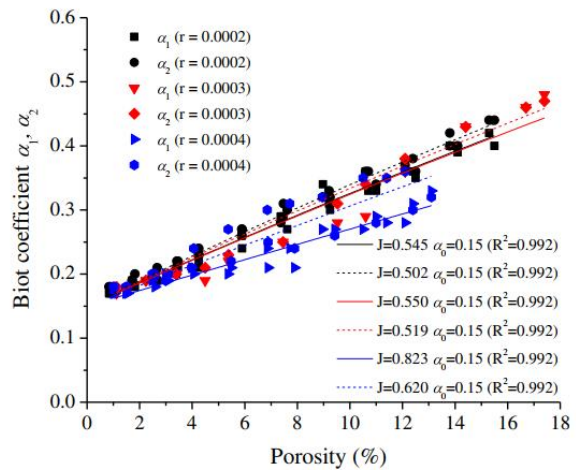
a) Random distributed circular pores with different porosity ($r=0.2\text{mm}$).



b) Random distributed circular pores with different porosity ($r=0.4\text{mm}$).



c) Isotropic Biot's coefficient vs. porosity



d) Anisotropic Biot's coefficients vs. porosity

Fig. 5.4: Influence of porosity on Biot-coefficient assuming randomly distributed circular pores (Tan & Konietzky 2014b)

One has to consider that the internal structure of rocks will change during the loading (poroelastic theory will be violated) due to microcrack growth and coalescence, pore deformation or closure etc. This leads to a change in the Biot value as function of stress and strain, respectively, as illustrated by Fig. 5.5. Deformations up to point D are characterized by pore and microcrack closure, later on crack evolution takes place and leads to increase in pore volume.

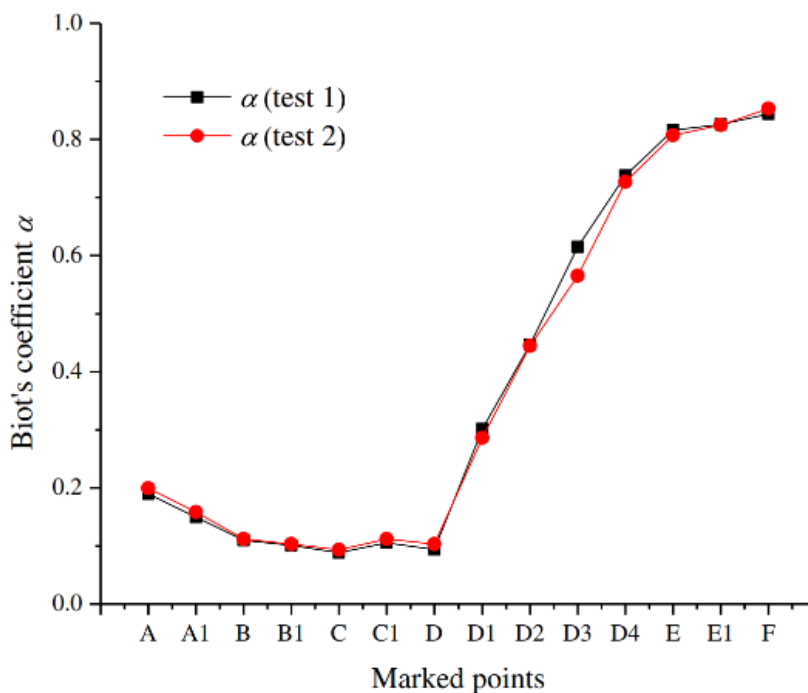
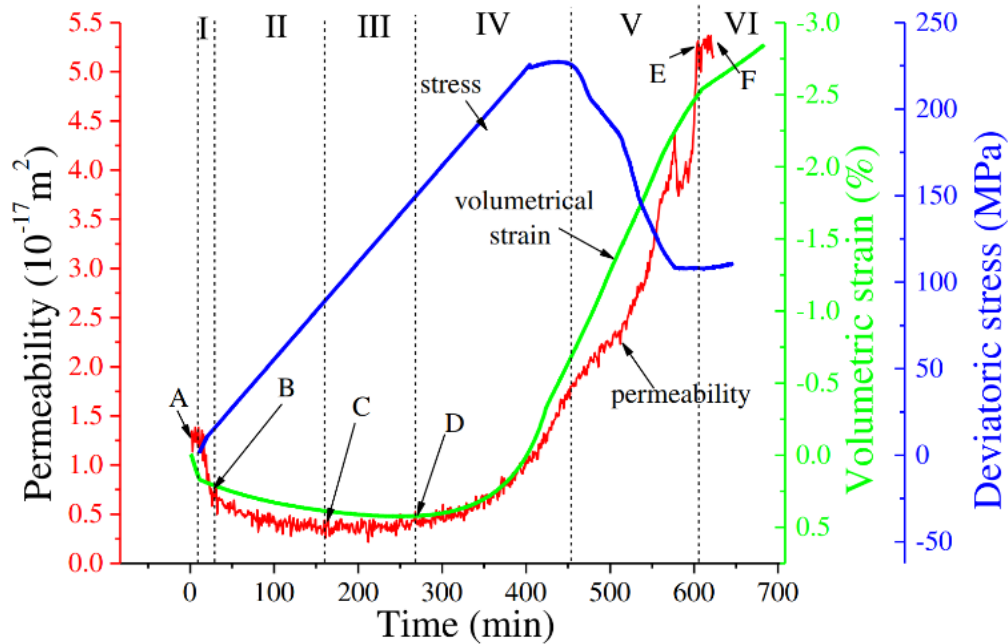


Fig. 5.5: Change of Biot-coefficient as function of deformation (Tan, Konietzky & Frühwirt, 2014a)

Another often used parameter is Skempton's coefficient B (lies also between 0 and 1), which is measured under undrained loading conditions:

$$B = \frac{\Delta p p}{\Delta \sigma^{iso}} = \frac{\alpha}{\alpha^2 + K_s \cdot S} \quad (5.4)$$

where $\Delta p p$ is the increment of pore water pressure and $\Delta \sigma^{iso}$ is the increment of the increase in isotropic stress, respectively.

In respect to stability and failure one has to consider that fluid pressure will reduce the effective stresses. As illustrated in Fig. 5.6 this means a shift of Mohr's circle to the left, which reduces safety.

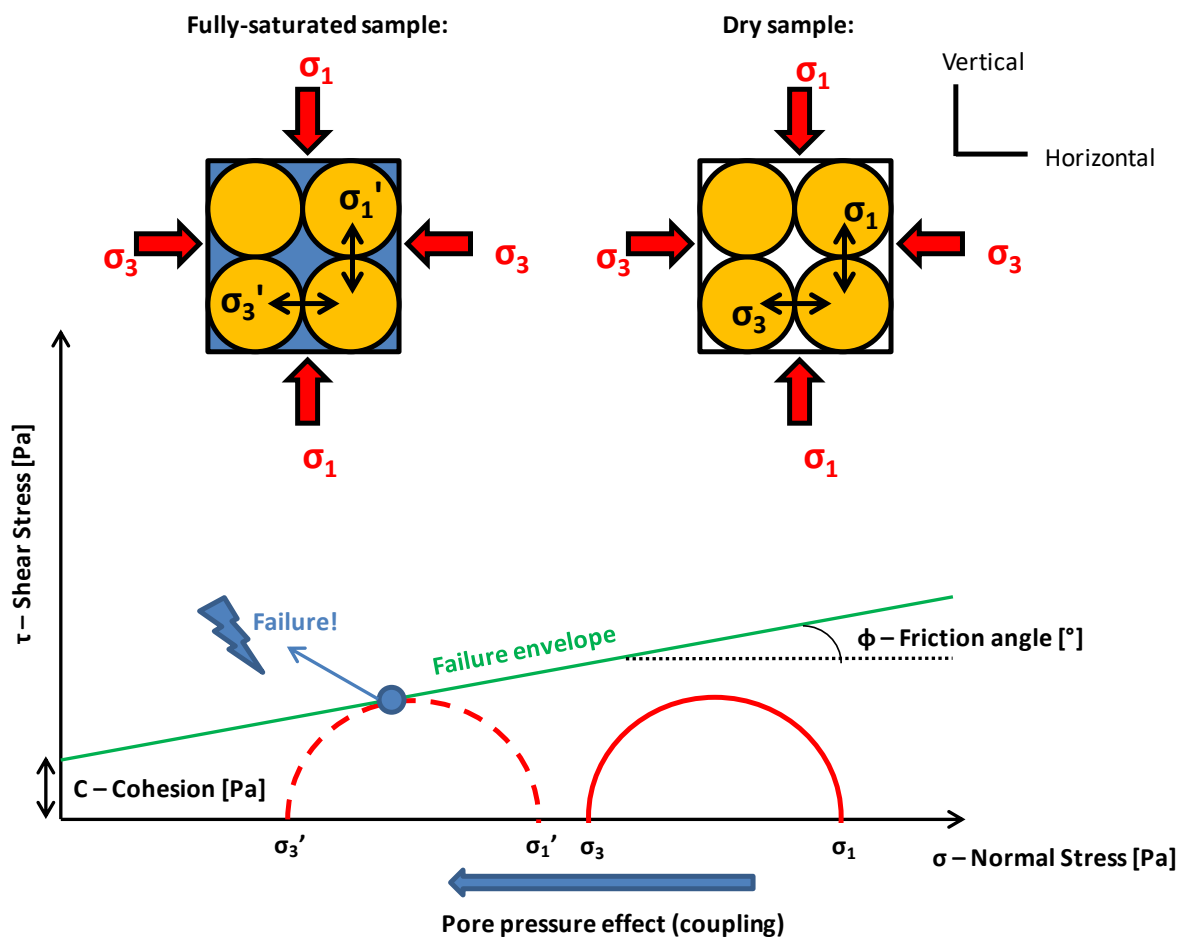


Fig. 5.6: Illustration of the effective stress concept

The probably best and most comprehensive description of the poroelastic theory is given by Detournay and Chen (1993).

6 Permeability and porosity determination

Permeability and porosity can be determined either by field tests (especially by bore-hole testing) or investigations on cores in the lab. This chapter deals only with lab testing.

The total porosity n_{total} can be determined as the ratio between grain density and bulk density:

$$n_{\text{total}} = 1 - \frac{\rho^{\text{bulk}}}{\rho^{\text{grain}}} \quad (6.1)$$

Pores are classified according to their size into four groups (Tab. 6.1).

Open porosity can be determined by the following methods:

- mercury porosimetry: based on wetting characteristics of mercury and suited for small pores in nanometre and micrometre range
- Gas expansion method: based on volume and pressure balance in two chambers, one of them with rock sample
- Imbibition method with water (suited for macropores): based on weight difference between dry and fully saturated sample

The mercury porosimetry allows - by applying different pressure levels – the determination of the pore size distribution. Also, X-ray tomography or optical methods based on thin slices can be used to determine the porosity and pore size distribution.

It has to be distinguished between gas and liquid permeability. For gases the so-called Klinkenberg effect (slippage of gas at grain surfaces which leads to higher flow rates) has to be considered (see chapter 2). Due to this effect gas permeability is always greater than fluid permeability.

To determine liquid permeability the following two test methods are common:

- permeability test with water under constant hydraulic pressure difference, measuring flow rate under stationary conditions and evaluation according to Darcy's law (e.g. Tan, Konietzky & Frühwirt 2014a)
- puls decay method: based on the decay of water pressure suddenly applied to a rock sample (e.g. Jones 1997; Tan, Konietzky & Frühwirt 2014a)

Tab. 6.1: Pore classification according to diameter (Sperl & Trckova, 2008)

Pore class	Diameter range / nm
Micropores	$d < 2$
Mesopores	$2 < d < 50$
Macropores	$50 < d < 7500$
Rough pores	$d > 7500$

Hydraulic borehole tests (head tests) are the most common techniques to determine the permeability in-situ. The most popular and easy to perform test is the so-called Lugeon-test like illustrated in Fig. 6.1.

More detailed information about different hydraulic borehole tests including their set-up and evaluation are given for instance by Das (1987).

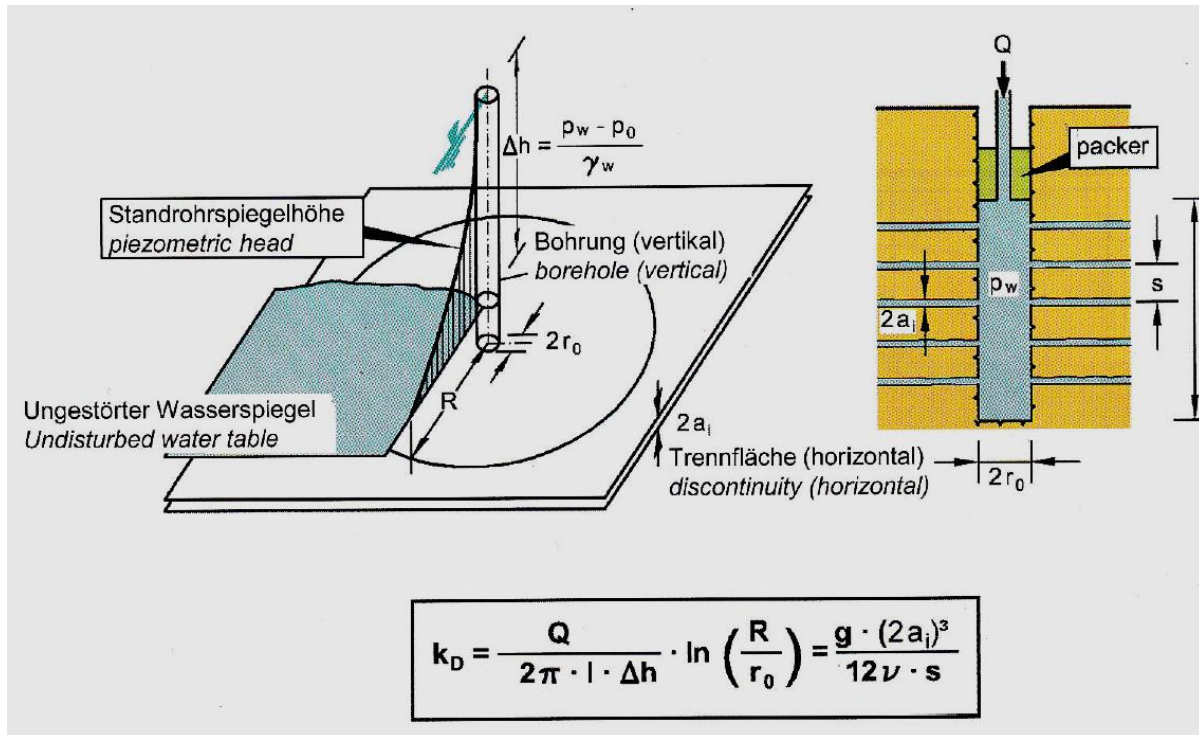


Fig. 6.1: Spatial configurations of water and air in a porous material (Wittke et al., 2021)

7 Two-phase flow

Besides the already discussed single phase flow, also two phase flow is of importance, especially in form of gas-fluid mixture or mixture of different fluids like water and oil. The different phases can be either dissolved in each other or they exist as immiscible fluids separated by interfaces (no evaporation and no dissolution). The latter one – especially water and air - will be considered here, because it is of major practical importance for geotechnical engineering.

Fig. 7.1 illustrates the possible different spatial configurations:

- a) absorbed regime: tight bonded water at the rock/soil grains, water is immobile
- b) capillary pendular regime: less tight bonded water, occurs in isolated regions, water does not create continuous flow paths, water is nearly immobile
- c) capillary funicular regime: regions of pendular water coalesce, continuous water flow possible
- d) occluded air bubble regime: water films becomes thicker, pores become completely water filled, air phase losses its continuity, only single air bubbles exist
- e) fully saturated regime: full water saturation is reached

The two-phase flow discussed below considers the states c to e according to Fig. 7.1.

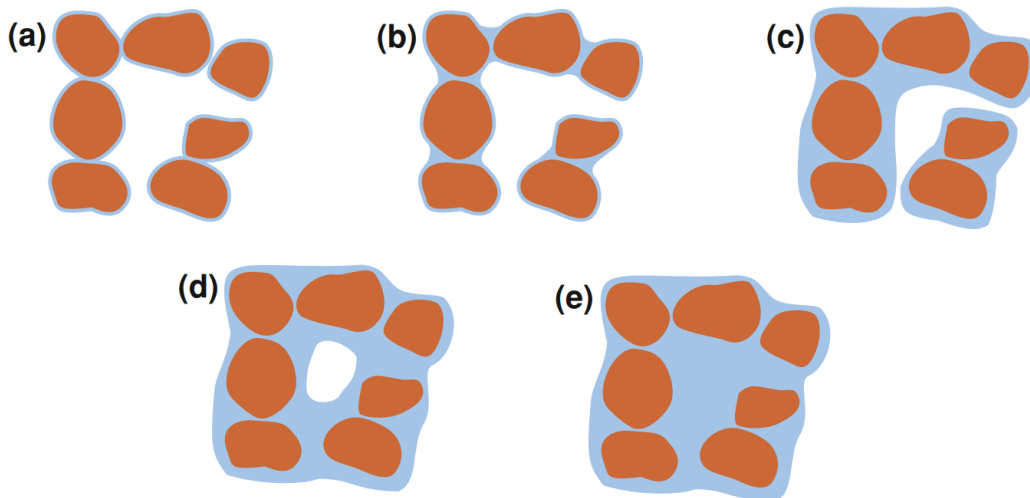


Fig. 7.1: Spatial configurations of water and air in a porous material (Szymkiewicz, 2013)

According to the attraction of the fluid phase by the surface of the rock/soil skeleton, the phases are called ‘wetting phase’ (= water) or ‘non-wetting phase’ (= air). According to Fig. 7.2c the pressure difference (= capillary pressure) between the water and air phase considering two spherical particles is given by the so-called Laplace equation:

$$\Delta P = P_{nw} - P_w = \sigma_{aw} \cdot \left(\frac{1}{r_{c1}} + \frac{1}{r_{c2}} \right) \quad (7.1)$$

where σ_{aw} is the surface tension of the air-water interface (app. 0.072 N/m at room temperature; please note, that surface tension decreases with increasing temperature).

If a tube is considered as a simplified flow channel the capillary pressure is given by the following equation (see Fig. 7.2b):

$$\Delta P = P_c = P_{nw} - P_w = \frac{2\sigma_{aw} \cos(\psi)}{r_c} \quad (7.2)$$

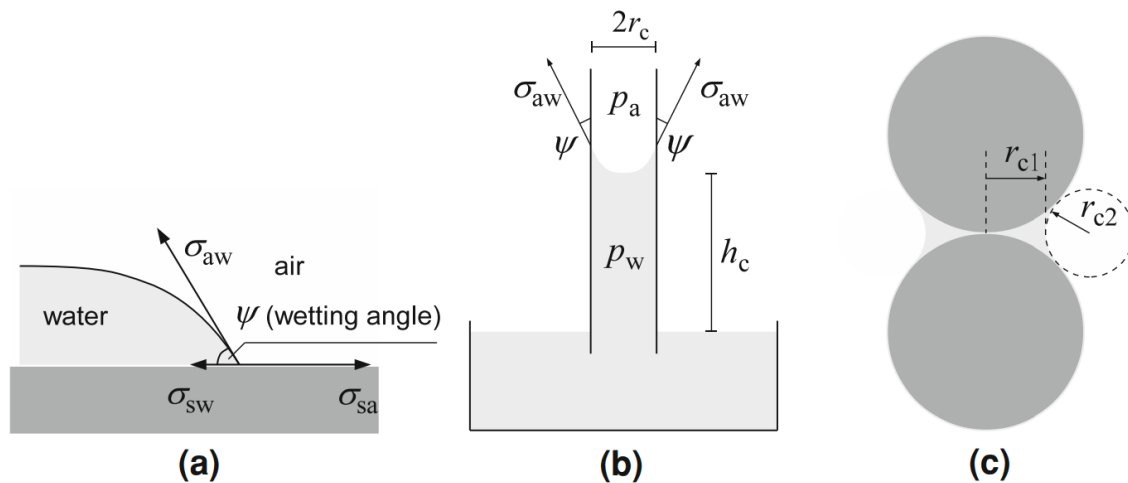


Fig. 7.2: Illustration of the pressure concept between two immiscible fluid phases (Szymkiewicz, 2013)

Under assumption of (a) room temperature and (b) tube is perfect wetting (wetting angle = 0°), the capillary rise is given by the following formula (see also Fig. 7.2a,b):

$$h_c = \frac{1.5 \cdot 10^{-5}}{r_c} \quad (7.3)$$

Please note, that h_c and r_c are given in m.

The relation between saturation and capillary pressure is described by the so-called capillary function (= suction function or retention function), see Fig. 7.4. If air (gas) want to enter a saturated or partially saturated medium the so-called ‘entry-pressure’, has to be exceeded. The air entry pressure s_{AE} (see Fig. 7.3) is obtained by intersecting the horizontal line at degree of saturation equal to unity with the line tangent to the curve at the inflection point.

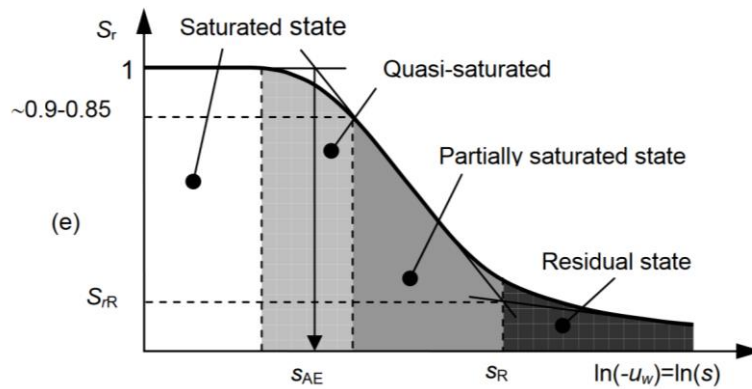


Fig. 7.3: Illustration of saturation phases vs. suction pressure (Tarantino, 2013)

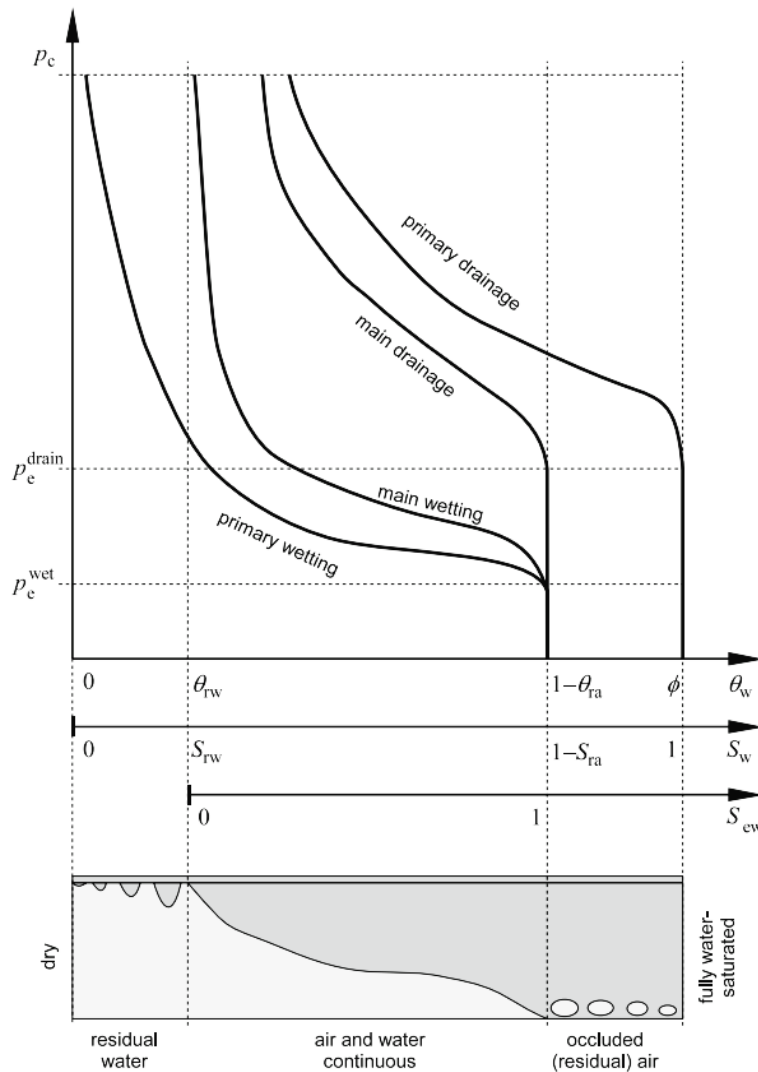


Fig. 7.4: Capillary pressure-water saturation relationship for different water and air regimes, where the subscripts are: w=water, a=air, r=residual, e=entry, c=capillary and the symbols are: p=pressure, S=saturation; Θ =volume fraction; 'drainage' means transition from saturated to dry state and 'wetting' means the opposite (Szymkiewicz, 2013)

Two-phase flow can be described by an extension of Darcy's law by introducing individual relative permeabilities k_r for each phase (wetting phase with subscript 'w' and non-wetting phase with subscript 'nw'):

$$q_w = \frac{K \cdot k_{rw}}{\mu_w} \frac{\partial P_w}{\partial l} \quad (7.4)$$

$$q_{nw} = \frac{K \cdot k_{rnw}}{\mu_{nw}} \frac{\partial P_{nw}}{\partial l} \quad (7.5)$$

The difference between the pressure of the non-wetting and the wetting phase is called capillary pressure P_c :

$$P_c = P_{nw} - P_w \quad (7.6)$$

The relative permeabilities are functions of the phase saturations, whereby for the saturations S the following holds:

$$1 = S_w + S_{nw} \quad (7.7)$$

The effective saturation S_e is given by the following relation:

$$S_e = \frac{S_w - S_{w,residual}}{1 - S_{w,residual}} \quad (7.8)$$

For the relative permeabilities certain functions have to be specified. The most popular relations are given by the so-called Van-Genuchten law:

$$k_{rw} = S_e^a \left[1 - (1 - S_e^{1/b})^b \right]^2 \quad (7.9)$$

$$k_{rnw} = (1 - S_e)^c \left[1 - S_e^{1/b} \right]^{2b} \quad (7.10)$$

where a , b and c are constants which have to be determined by lab or field tests. The capillary pressure is a function of the saturation of the wetting phase and is given according to the Van-Genuchten law as follows (P_0 is a constant):

$$P_c = P_0 \left[S_e^{-1/b} - 1 \right]^{1-b} \quad (7.11)$$

Exemplary, Fig. 7.5 shows relations obtained from lab tests, which follow quite closely the above given relations based on the van-Genuchten law and could be fitted by them. The bulk density of the rock has to consider the dry density of the rock and partially the densities of the two fluid phases according to their partial saturations under consideration of the porosity:

$$\rho_{bulk} = \rho_{rock, dry} + n \cdot (S_w \rho_w + S_{nw} \rho_{nw}) \quad (7.12)$$

The average pore water pressure which has to be considered in effective stress calculations can be obtained by the following expression:

$$pp = S_w P_w + S_{nw} P_{nw} \tag{7.13}$$

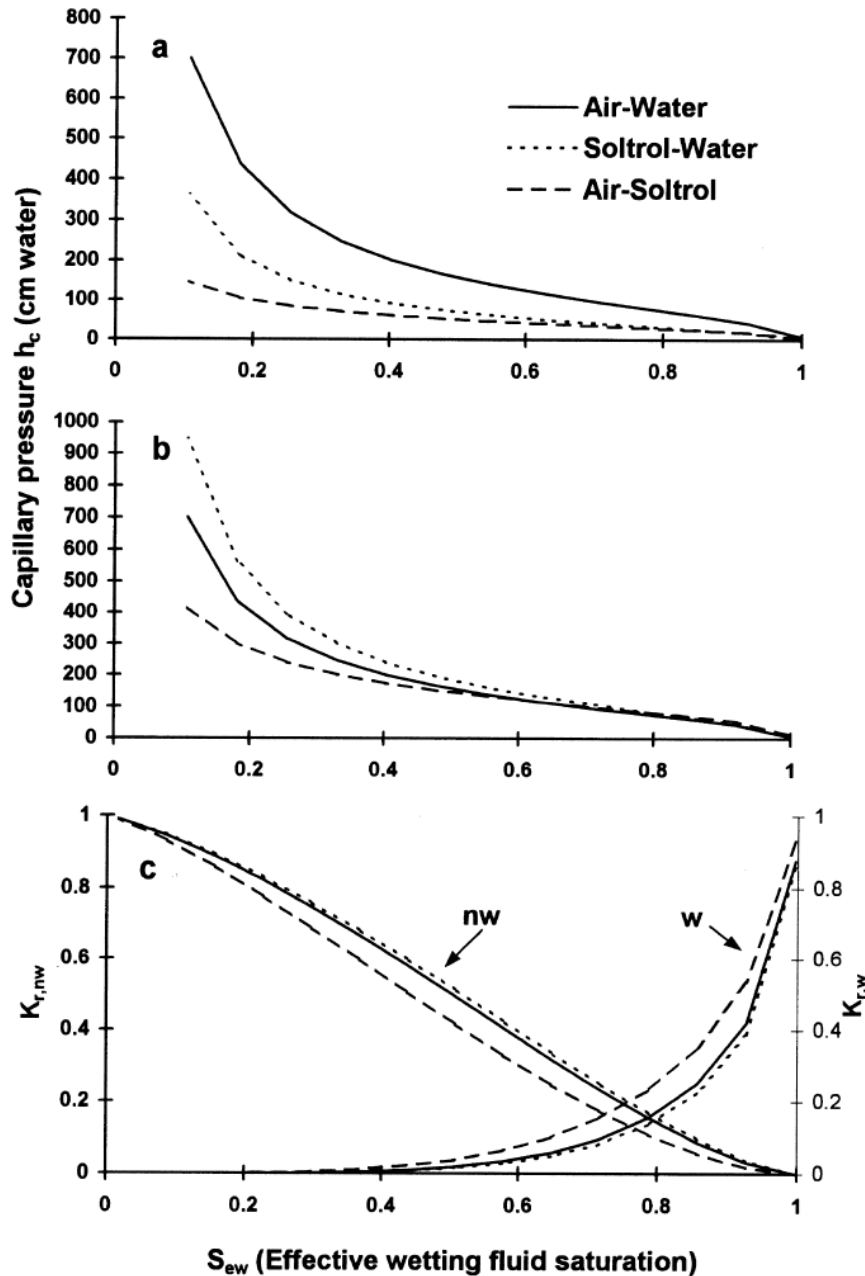


Fig. 7.5: Capillary pressure (a: unscaled; b: scaled) and relative permeabilities (c) for two-phase flow in Columbia soil (Chen et al. 1999)

Exemplary, Fig. 7.6 shows the saturation and hydraulic conductivity for two different geomaterials: sand and silt. It becomes visible, that suction pressure in certain geomaterials can reach quite high values up to several MPa. This has significant mechanical implications like the creation of apparent cohesion.

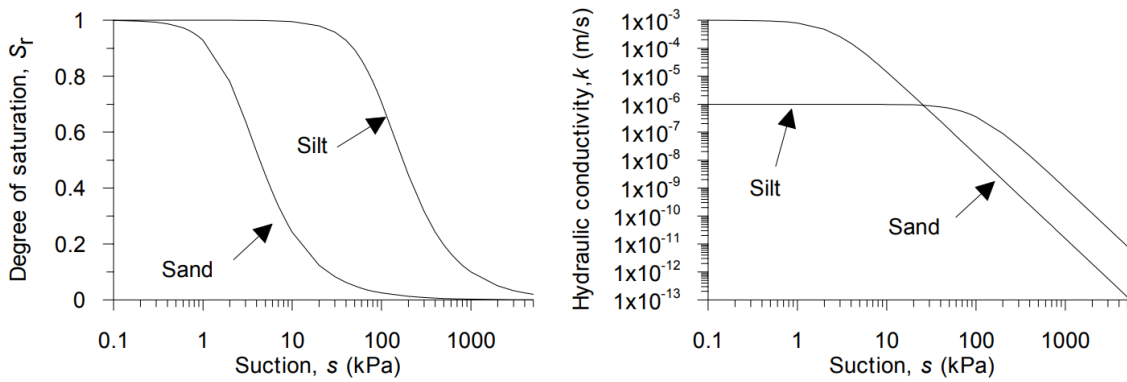


Fig. 7.6: Hydraulic conductivity vs. suction (= capillary pressure) for silt and sand (Tarantino, 2013)

The extended Darcy equation considering two-phase flow leads to two coupled partial differential equations:

$$\frac{\partial}{\partial t} [\rho_w(P_w) S_w n] - \nabla \left[\frac{\rho_w(P_w) k_{rw}(S_w) k_s}{\mu_w} (\nabla P_w - \rho_w(P_w) g) \right] = 0 \quad (7.14)$$

$$\frac{\partial}{\partial t} [\rho_{nw}(P_w, S_w) (1 - S_w) n] - \nabla \left[\frac{\rho_{nw}(P_w, S_w) k_{rnw}(S_w) k_s}{\mu_{nw}} (\nabla P_w - \nabla P_c(S_w) - \rho_{nw}(P_w, S_w) g) \right] = 0$$

where: k_s is the permeability tensor (max. perm.) and g is the gravity vector. All other symbols are already explained above.

These extended Darcy equations (7.14) for two-phase flow (coupled differential equations) can be simplified by considering that air viscosity is much smaller than water viscosity and that pore air pressure is equal to atmospheric pressure, so that equation for air flow can be neglect. If one further neglect water compressibility and spatial gradients of water density, the so-called Richards equation (single differential equation) can be obtained, which is often used to simulate water flow in partial and saturated geomaterials (C is the storage coefficient):

$$\frac{\partial P_w}{\partial t} C(P_w) - \nabla \left[\frac{k_{rw} k_s}{\mu_w} \nabla (P_w - \rho_w g) \right] = 0 \quad (7.15)$$

8 Further geohydraulic problems

The chapters above have just touched a few fundamentals, some further advanced topics are listed below:

- Multi-phase flow
 - Immiscible or miscible fluids
 - Two-Phase flow (e.g. water and air), Three-Phase flow (e.g. water, oil and gas)
- Double porosity
 - Flow through fractures and porous matrix
- Unsaturated flow
 - Phreatic surface
 - Partial saturation
 - Capillary forces
- Discrete Fracture Networks (DFN)
 - Hydraulic and HM-coupled simulations
- Dynamic pore and joint water generation
 - Seismic excitation (earthquakes, explosions etc.)
- Chemical coupling
 - Transport modelling
 - HC-coupling
 - HTMC-coupling
- Hydraulic fracturing
 - Hydraulic fracture propagation
 - Leak-off
- CO₂-Sequestration and reservoir engineering in general
- Injections to reduce permeability and/or increase strength
- Leaching to extract minerals

9 Literature

- Aadnoy, B.S. & Looyeh, R. (2011): Petroleum rock mechanics, Gulf Professional Publishing
- Achtziger-Zupancic, P. et al. (2017): A new global database to improve predictions of permeability distribution in crystalline rocks at the site scale, *Journal of Geophysical Research: Solid Earth*, 122: 3513-3539
- Bear, J. (1972): Dynamics of Fluids in Porous Media, American Elsevier, New York
- Blytt, H.H. (2017): An experimental and numerical study of diffusion and electrical conductivity in porous media, Master Thesis, NTNU
- Chen, J., Hopmans, J.W. & Grismer, M.E. (1999): Parameter estimation of two-fluid capillary pressure-saturation and permeability functions, *Advances in Water Resources*, 22(5): 479-493
- Das, B.M. (1987): Advanced Soil Mechanics, McGraw Hill International Editions
- Detournay, E. & Cheng, A. (1993): Fundamentals of Poroelasticity, in: *Comprehensive Rock Engineering*, Vol II, Chapter 5, Pergamon Press, 113-171
- Domenico, P.A. & Schwartz, F.W. (1990): Physical and Chemical Hydrogeology, John Wiley & Sons, New York
- Finenko, M. & Konietzky, H. (2017): CFD-Simulations for water flow through fractures, TU BAF, Geotechnical Institute, internal unpublished report
- Finenko, M. & Konietzky, H. (2021): Hausdorff distance as a 3D fracture aperture metric, *Rock Mech. Rock Eng.*, 54: 2355-2367
- Finenko, M. & Konietzky, H. (2024a): Numerical simulation of turbulent fluid flow in rough rock fracture: 2D case, *Rock Mech. Rock Eng.*, 57: 451-479
- Finenko, M. & Konietzky, H. (2024b): Numerical simulation of turbulent fluid flow in rough rock fracture: 3D case, *Rock Mech. Rock Eng.*, 57: 2297-2323
- Freeze R. A., Cherry J. A. (1979): Groundwater, Prentice-Hall International, New Jersey
- Javadi, M. et al. (2014): Critical Reynolds number for nonlinear flow through rough-walled fractures: The role of shear process, *Water Resources Research*, 50: 1879-1804
- Jones, S.C. (1997): A technique for faster puls-decay permeability measurements in tight rocks, SPE-28450-PA
- Ranjith, P.G. & Darlington, W. (2007): Nonlinear single-phase flow in real rock joints, *Water Resources Research*, 43: W09502
- Rushing, J.A. et al. (2004): Klinkenberg-corrected permeability measurements in tight gas sands: steady-state versus unsteady-state techniques, SPE 89867
- Sjoberg, A. et al. (2010): Measurement methods for stored VOC in concrete floors, Nordic Concrete Research
- Sperl, J. & Trčková, J. (2008): Permeability and porosity and their relationship based on laboratory testing, *Acta Geodyn. Geomater.*, 149: 41-47
- Szymkiewicz, A. (2013): Modelling water flow in unsaturated porous media, *Geo-Planet: Earth and Planetary Sciences*, Springer, 238 p.

- Tan, X.; Konietzky, H.; Frühwirt, T. (2014a): Laboratory observation and numerical simulation of permeability evolution during progressive failure of brittle rocks, *Int. J. Rock Mech. Mining Sci.*, 68: 167-176.
- Tan, X. & Konietzky, H. (2014b): Numerical study of variation in Biot's coefficient with respect to microstructure of rocks, *Tectonophysics*, 610: 159-171
- Tan, X.; Konietzky, H.; Frühwirt, T. (2015): Experimental and Numerical Study on evolution of Biot's Coefficient during Failure Process for Brittle Rocks, *Rock Mechanics Rock Engineering*, 48: 1289-1296.
- Tarantino, A. (2013): Basic concepts in the mechanics and hydraulics of unsaturated geomaterials, 3-28, doi.10.1002/9781118616871.ch1.
- UTAH (2020): <https://my.eng.utah.edu/~lzang/images/lecture-4.pdf>
- Wittke, M. et al. (2021): Design and construction of tunnels in jointed rock according to ajrm method – part 2, *tunnel*, 4: 22-35
- Zimmerman, R.W. et al. (2004): Non-linear regimes of fluid flow in rock fractures, Paper 1A 27, *Proc. SINOROCK_2004*